EAVN Status Report for the 2020B Semester

EAVN User Support Team, NAOJ, SHAO, XAO, and KASI

April 27, 2020

Major revision since the 2020B semester

- Number of VERA antennas will be reduced due to the shutdown of IRK, OGA, and ISG stations (see Appendix).
- New observing mode (K/Q-band simultaneous data reception) is available at KaVA and Nobeyama (see Section 3 and Appendix)

Contents

1	Intr	oducti	ion						
2	Sys	tem							
	2.1	Array							
	2.2	Anten	nas						
		2.2.1	Brief Summary of VERA Antennas						
		2.2.2	Brief Summary of KVN Antennas						
		2.2.3	Nobeyama 45-m Telescope						
		2.2.4	Takahagi 32-m Telescope						
		2.2.5	Tianma 65-m Telescope						
		2.2.6	Nanshan 26-m Telescope						
		2.2.7	Aperture Efficiency						
		2.2.8	Beam Pattern and Size						
	2.3	Receiv	vers						
		2.3.1	Brief Summary of VERA Receiving System						
		2.3.2	Brief Summary of KVN Receiving System						
		2.3.3	Brief Summary of NRO45 Receiving System						
		2.3.4	Brief Summary of TAK32 Receiving System						
		2.3.5	Brief Summary of TMRT65 Receiving System						
		2.3.6	Brief Summary of NSRT26 Receiving System						
	2.4	Digita	l Signal Processing						
	2.5	Record	ders						
	2.6	Correlators							
		2.6.1	Note for the C2 mode						
	2.7	Calibr	ation						
		2.7.1	Delay and Bandpass Calibration						
		2.7.2	Gain Calibration						
	2.8	Geode	etic Measurement						
		2.8.1	Brief Summary of VERA Geodetic Measurement						
		2.8.2	Brief Summary of KVN Geodetic Measurement						
3	Obs	erving	; Proposal						
	3.1	Call fo	or Proposals (CfP)						
	3.2	Proposal Submission							
	3.3	Specia	d Condition for Selecting Proposals						
	3.4	Observ	vation Mode						
	3.5	Possib	ble Conflict/Duplication with KaVA/EAVN Large Programs						

	3.6	Target	t of Opportunity (ToO) Observations	28					
	3.7	Angular Resolution and Largest Detectable Angular Scale							
	3.8	Sensit	ivity	29					
	3.9	Calibr	ator Information	30					
	3.10	Data .	Archive	31					
4	Not	es for	special modes	32					
	4.1	Phase	-referencing and astrometry	32					
		4.1.1	Fast switching	32					
		4.1.2	Separation angle between target and phase reference	32					
		4.1.3	Tropospheric calibration with GPS or JMA or Geodetic blocks .	32					
		4.1.4	Astrometric accuracy	33					
		4.1.5	Baseline length	35					
		4.1.6	A priori model of the KJCC correlator	35					
		4.1.7	Data reduction	35					
	4.2	1-bear	m hybrid $(K/Q/W)$ mode	36					
	4.3	Wide-	field imaging mode	37					
	4.4	Simul	taneous K/Q band mode	37					
5	Obs	ervati	on and Data Reduction	38					
	5.1	Prepa	ration of an EAVN Observation	38					
	5.2	Obser	vation and Correlation	38					
	5.3	Data	Reduction	36					
	5.4	Furthe	er Information	39					
\mathbf{A}	Effe	ct of t	the reduction of the VERA antennas	39					
	A.1	Case 1	1: KaVA imaging of H ₂ O masers in high-mass star-forming region	39					
	A.2	Case 2	2: KaVA Imaging of a Continuum Source	43					
	A.3	3 Case 3: KaVA and EAVN astrometry							

1 Introduction

This document describes the current observational capabilities as of 2020 April, and available observing time of the East Asian VLBI Network (EAVN). EAVN is the international collaborative VLBI array operated by Korea Astronomy and Space Science Institute (KASI), National Astronomical Observatory of Japan (NAOJ), Shanghai Astronomical Observatory (SHAO; China), and Xinjiang Astronomical Observatory (XAO; China).

EAVN invites proposals for open-use observations to be carried out from September 1 2020 to January 15, 2021 (2020B semester). The total observing time of 500 hours is provided for EAVN open-use operation to proposers, while the available machine time of each telescope is different between each other. Please refer to Section 3 for more details.

In the 2020B semester, EAVN is operated using 8 telescopes, 1 telescope of VERA, Nobeyama 45-m and Takahagi 32-m telescopes in Japan, 3 telescopes of KVN in Korea, Tianma 65-m and Nanshan 26-m telescopes in China. Note that the number of VERA antennas is reduced from 4 to 1 due to the shutdown of the Iriki, Ogasawara, and Ishigakijima stations. see the following web site for details.

http://www.miz.nao.ac.jp/en/content/news/topic/20200327-382

Figure 1 shows location of EAVN telescopes which participate in open-use observations of EAVN in the 2020B semester.

This status report summarizes general information about EAVN brief summary and the performance of each telescope/array, and how to prepare and submit proposals for EAVN.



Figure 1: Location of EAVN sites, including the Korea-Japan Correlation Center at KASI, Korea, overlaid on 'the Blue Marble' image (credit of the ground image: NASA's Earth Observatory). Note that only one stations in VERA (Mizusawa) will join the EAVN observations in 2020B, but the others (Iriki, Ogasawara, and Ishigakijima) will not be available.

2 System

2.1 Array

In the 2020B semester, 8 radio telescopes (KVN 3 × 21 m, VERA 20 m at Mizusawa, Nobeyama 45 m, Takahagi 32 m, Tianma 65 m, and Nanshan 26 m) are available for EAVN open use, as shown in Figure 1. Note that the number of VERA antennas is reduced from 4 to 1 due to the shutdown of the Iriki, Ogasawara, and Ishigakijima stations. In this section, we leave the information about VERA Iriki, Ogasawara, and Ishigakijima stations just for references (Tables 1, 2, and 4). Takahagi 32 m telescope newly participates in EAVN open-use program from the 2020A semester. Two observing frequencies, 22 (K-band) and 43 GHz (Q-band), are opened in the 2020B semester.

KaVA (KVN and VERA Array) is a core array of EAVN, which consists of 4 antenna sites in VERA-Mizusawa, KVN-Yonsei, KVN-Ulsan and KVN-Tamna with 6 baselines in 2020B. The maximum baseline length of the KaVA in 2020B is 1464 km between Mizusawa and Tamna (although Mizusawa-Ishigakijima baseline is 2270 km), and the minimum baseline length is 305 km between Yonsei and Ulsan. The maximum angular resolution expected from the baseline length of KaVA (2270 km) is about 1.2 mas for K-band and about 0.6 mas for Q-band, although they are expected to be degraded to about 2.0 mas and 1.0 mas, respectively, for the Mizusawa—Tanma baseline. The maximum angular resolution was improved to be 0.55 mas at K-band for EAVN (the longest baseline of 5100 km for VERA-Ogasawara - Nanshan baseline), and that at Q-band was identical to that of VERA (0.63 mas for VERA-Mizusawa – VERA-Ishigakijima baseline) for the full-array of EAVN until the last semester 2020A. However, the maximum angular resolutions will be 0.65 mas for the K-band (corresponding to the longest baseline of 4375 km between the VERA-Mizusawa – Nanshan baseline) and 0.70 mas at the Q-band (corrensponding to the longest baseline of 1986 km between the VERA-Mizusawa – Tianma baseline) in 2020B. The geographic locations and coordinates of EAVN antennas in the coordinate system of epoch 2009.0 are summarized in Table 1. Figures 2 and 3 show examples of uv plane coverage for KaVA and EAVN, respectively.

The coordinates and averaged velocities of KaVA sites in Table 2 are predicted values at the epoch of January 1, 2018. Reference frame of these coordinates is ITRF2014. The rates of the coordinates of Mizusawa, Iriki, Ogasawara and Ishigakijima are the average value of change of the coordinates from April 16, 2016 to May 26, 2018, after the 2016 Kumamoto Earthquake ($M_j = 7.3$). The 2011 off the Pacific coast of Tohoku Earthquake ($M_j = 9.0$) brought the co-seismic large step and non-linear post-seismic movement to the coordinates of Mizusawa. Co-seismic steps of the coordinates of Mizusawa are dX = -2.0297 m, dY = -1.4111 m and dZ = -1.0758 m. The creeping continues still now, though decreased. The changes of coordinates by the post-seismic creeping are dX = -1.2148 m, dY = -0.6402 m and dZ = -0.3042 m in total from March 12, 2011 to January 1, 2020.

The antenna positions of KVN are regularly monitored by geodetic VLBI observations in collaboration with VERA.

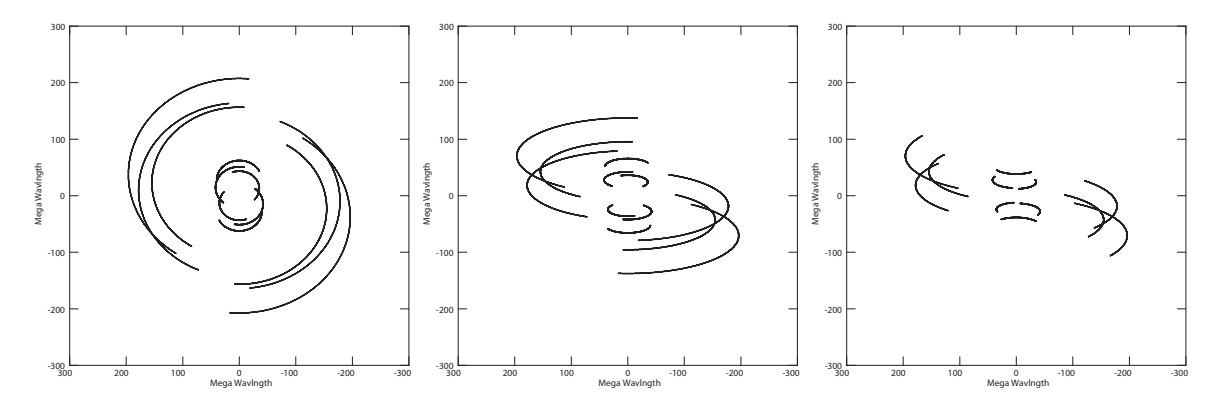


Figure 2: Examples of (u, v) coverage for a KaVA observation at 43 GHz with the source's declination of $+60^{\circ}$ (left panels), $+20^{\circ}$ (center panels), and -20° (right panels). Four antennas (KVN 3 stations and VERA Mizusawa) will be available in the 2020B semester. Total observation duration of 10 hours and the antenna's lower elevation limit of 15° are assumed for all cases.

2.2 Antennas

2.2.1 Brief Summary of VERA Antennas

All the telescopes of VERA have the same design, being a Cassegrain-type antenna on AZ-EL mount. Each telescope has a 20 m diameter dish with a focal length of 6 m, and with a sub-reflector of 2.6 m diameter. The dual-beam receiver systems are installed at the Cassegrain focus. Two receivers are set up on the Stewart-mount platforms, which are sustained by steerable six arms, and with such systems one can simultaneously observe two adjacent objects with a separation angle between 0.32 and 2.2 deg. The whole receiver systems are set up on the field rotator (FR), and the FR rotate to track the apparent motion of objects due to the earth rotation. Table 3 summarizes the ranges of elevation (EL), azimuth (AZ) and field rotator angle (FR) with their driving speeds and accelerations. In the case of single beam observing mode, one of two beams is placed at the antenna vertex (separation offset of 0 deg).

2.2.2 Brief Summary of KVN Antennas

The KVN antennas are also designed to be a shaped-Cassegrain-type antenna with an AZ-EL mount. The telescope has a 21 m diameter main reflector with a focal length of 6.78 m. The main reflector consists of 200 aluminum panels with a manufacturing surface accuracy of about 65 μ m. The slewing speed of the main reflector is 3 °/sec, which enables fast position-switching observations (Table 3). The sub-reflector position, tilt, and tip are remotely controlled and modeled to compensate for the gravitational deformation of the main reflector and for the sagging-down of the sub-reflector itself.

2.2.3 Nobeyama 45-m Telescope

The Nobeyama 45-m Telescope (hereafter NRO45) is one of the largest millimeter radio telescope in the world. It has a Cassegrain-Coudé optics. The paraboloidal main reflector consists of about 600 pieces of panels, each of which has a surface accuracy of about 60 microns, and the deviation of the whole antenna from an ideal paraboloid is about 90 microns. The sub-reflector has a diameter of 4 m with a convex hyperboloid

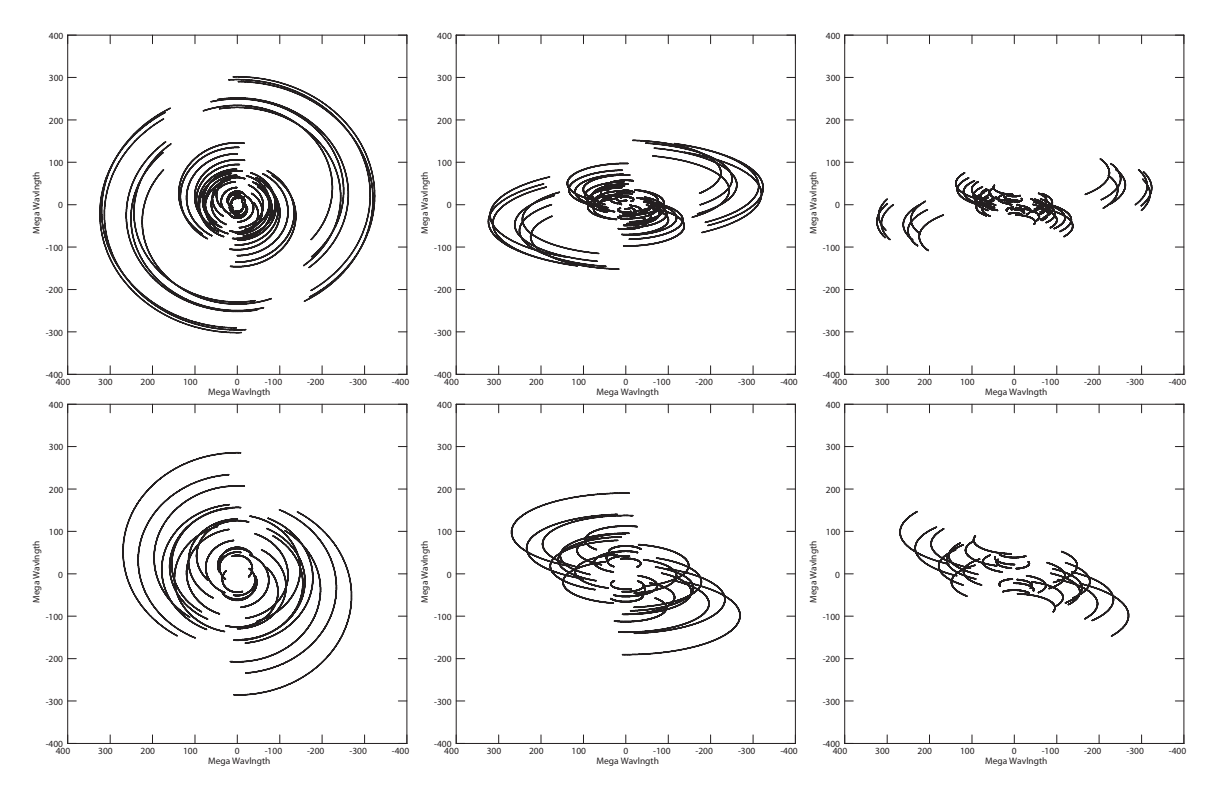


Figure 3: Examples of (u, v) coverage for an EAVN observation with full array configuration at 22 GHz (upper panels) and 43 GHz (lower panels) with the source's declination of $+60^{\circ}$ (left panels), $+20^{\circ}$ (center panels), and -20° (right panels). For K-band and Q-band, 8 and 6 antennas at maximum will be available in the 2020B semester. Total observation duration of 10 hours and the antenna's lower elevation limit of 15° are assumed for all cases.

surface, the position of which is computer-controlled to follow the moving focal point because the main reflector deforms as the elevation angle changes. The slewing speed of the telescope is 20°/min (i.e., 0.3°/sec). The (EL, AZ) driving ranges are also summarized in Table 3. More details on the NRO45 can be found in the Nobeyama Radio Observatory official website [2].

2.2.4 Takahagi 32-m Telescope

The Takahagi 32-m Telescope (hereafter TAK32) has a shaped Cassegrain-Coude-type design with a 32-m diameter main reflector and a 2.9-m sub-reflector on Az-El mount. The telescope was constructed in 1992. Cryogenically-cooled receivers at 2 frequency bands (6 – 9 GHz and 21 – 25 GHz) are equipped. The surface accuracy of the main reflector is < 0.64 mm rms at the antenna elevation angle of 35 deg, and 1.6 mm at other antenna elevation angles. The surface accuracy of the sub-reflector is < 0.2 mm rms. The slewing rates of the main reflector is 0.07 deg/sec, as shown in Table 3. The tentative value of aperture efficiency of TAK32 is 30% at K-band (see Table 4; [9]).

2.2.5 Tianma 65-m Telescope

The Tianma 65-m Telescope (hereafter TMRT65) has a shaped Cassegrain-type design with a 65-m diameter main reflector and a 6.5-m sub-reflector on Az-El mount. The main reflector consists of 1008 aluminum panels deploying an active surface control

Table 1: Geographic locations and motions of each EAVN antenna.

	•				
East	North	Ellipsoidal			
Longitude	Latitude	Height	X	Y	Z
[° ′ ′′]	[° ′ ′′]	[m]	[m]	[m]	[m]
138 28 21.2	35 56 40.9	1350	-3871025.4987	3428107.3984	3724038.7361
$140\ 41\ 41.0$	$36\ 41\ 54.6$	117.0	-3961881.8250	3243372.4800	3790687.4490
$121\ 08\ 09.4$	$31\ 05\ 31.6$	49.2	-2826708.6380	4679237.0440	3274667.5330
$87\ 10\ 40.4$	$43\ 28\ 15.6$	2029.4	228310.1700	4631922.7550	4367064.0740
141 07 57.3	39 08 00.7	116.6	-3857244.9731	3108782.9179	4003899.1695
$130\ 26\ 23.6$	$31\ 44\ 52.4$	573.6	-3521719.8813	4132174.6817	3336994.1132
$142\ 12\ 59.8$	$27\ 05\ 30.5$	273.1	-4491068.3826	3481545.2394	2887399.8018
$124\ 10\ 15.6$	$24\ 24\ 43.8$	65.1	-3263995.2619	4808056.3902	2619948.6347
$126\ 56\ 27.4$	$37\ 33\ 54.9$	139	-3042281.0183	4045902.6730	3867374.3296
$129\ 14\ 59.3$	$35\ 32\ 44.2$	170	-3287268.6453	4023450.1367	3687379.9886
$126\ 27\ 34.4$	$33\ 17\ 20.9$	452	-3171731.6665	4292678.5393	3481038.7880
	East Longitude [°'"] 138 28 21.2 140 41 41.0 121 08 09.4 87 10 40.4 141 07 57.3 130 26 23.6 142 12 59.8 124 10 15.6 126 56 27.4 129 14 59.3	East North Longitude [°'"] 138 28 21.2 35 56 40.9 140 41 41.0 36 41 54.6 121 08 09.4 31 05 31.6 87 10 40.4 43 28 15.6 141 07 57.3 39 08 00.7 130 26 23.6 31 44 52.4 142 12 59.8 27 05 30.5 124 10 15.6 24 24 43.8 126 56 27.4 37 33 54.9 129 14 59.3 35 32 44.2	East Longitude North Latitude Ellipsoidal Height [°'"] [°'"] [m] 138 28 21.2 35 56 40.9 1350 140 41 41.0 36 41 54.6 117.0 121 08 09.4 31 05 31.6 49.2 87 10 40.4 43 28 15.6 2029.4 141 07 57.3 39 08 00.7 116.6 130 26 23.6 31 44 52.4 573.6 142 12 59.8 27 05 30.5 273.1 124 10 15.6 24 24 43.8 65.1 126 56 27.4 37 33 54.9 139 129 14 59.3 35 32 44.2 170	East North Ellipsoidal Longitude Latitude Height X [°'"] [°'"] [m] [m] 138 28 21.2 35 56 40.9 1350 -3871025.4987 140 41 41.0 36 41 54.6 117.0 -3961881.8250 121 08 09.4 31 05 31.6 49.2 -2826708.6380 87 10 40.4 43 28 15.6 2029.4 228310.1700 141 07 57.3 39 08 00.7 116.6 -3857244.9731 130 26 23.6 31 44 52.4 573.6 -3521719.8813 142 12 59.8 27 05 30.5 273.1 -4491068.3826 124 10 15.6 24 24 43.8 65.1 -3263995.2619 126 56 27.4 37 33 54.9 139 -3042281.0183 129 14 59.3 35 32 44.2 170 -3287268.6453	East Longitude North Latitude Ellipsoidal Height X Y [°'"] [°'"] [m] [m] [m] 138 28 21.2 35 56 40.9 1350 -3871025.4987 3428107.3984 140 41 41.0 36 41 54.6 117.0 -3961881.8250 3243372.4800 121 08 09.4 31 05 31.6 49.2 -2826708.6380 4679237.0440 87 10 40.4 43 28 15.6 2029.4 228310.1700 4631922.7550 141 07 57.3 39 08 00.7 116.6 -3857244.9731 3108782.9179 130 26 23.6 31 44 52.4 573.6 -3521719.8813 4132174.6817 142 12 59.8 27 05 30.5 273.1 -4491068.3826 3481545.2394 124 10 15.6 24 24 43.8 65.1 -3263995.2619 4808056.3902 126 56 27.4 37 33 54.9 139 -3042281.0183 4045902.6730 129 14 59.3 35 32 44.2 170 -3287268.6453 4023450.1367

^aThe position was measured in late 2016.

Table 2: Station code and average velocity of each KaVA antenna.

Site	$IVS2^a$	$IVS8^b$	CDP^c	$\Delta X [m/yr]^d$	$\Delta Y [m/yr]^d$	$\Delta Z [m/yr]^d$
Mizusawa	Vm	VERAMZSW	7362	-0.0433	-0.0138	-0.0047
Iriki	Vr	VERAIRIK	7364	-0.0159	-0.0049	-0.0098
Ogasawara	Vo	VERAOGSW	7363	0.0363	0.0242	0.0119
Ishigakijima	V_{S}	VERAISGK	7365	-0.0303	-0.0003	-0.0486
Yonsei	Ky	KVNYONSE		-0.0121	-0.0042	-0.0052
Ulsan	Ku	KVNULSAN		-0.0117	-0.0072	-0.0028
Tamna	Kt	KVNTAMNA		-0.0169	-0.0012	-0.0024

^aIVS 2-characters code

system with 1104 actuators. The prime mirror achieves a surface accuracy of about 0.3 mm rms after compensating the gravitational deformation in real time by the active surface control system. The secondary mirror has a surface error of 0.1 mm rms. A rotatable receiver cabin with the feeds covering frequency range from S-band (2 GHz) to Q-band is mounted at the Cassegrain focus, while the L-band (1.6 GHz) feed is off focus mount separately. The slewing rates of the main reflector are 0.5°/sec in azimuth and 0.3°/sec in elevation, as shown in Table 3. An overhead time of 10 seconds is recommended to settle the antenna on source.

Dual-beam receivers are installed in TMRT65 at both K- and Q-bands. These two beams have a fixed separation angle of 140 arcsec at K-band and 100 arcsec at Q-band. One of the beams is placed at the antenna focus for VLBI observations. The measured beam sizes (HPBW) are listed in Table 4.

^bThe position was measured in November 2015.

^cThe epoch of the coordinate is January 1, 2014.

^dThe epoch of the coordinates is January 1, 2019.

 $[^]b {
m IVS}$ 8-characters code

^cCDP (NASA Crustal Dynamics Project) code

^dThe epoch of the coordinates is January 01, 2018. Average speed was obtained from the VLBI data from January 01, 2018 to January 1, 2019.

2.2.6 Nanshan 26-m Telescope

The Nanshan 26-m Telescope (hereafter NSRT26) has a Cassegrain-type design with a 26-m diameter main reflector and a 3-m sub-reflector on Az-El mount. The telescope was constructed in 1993 with 25-m-diameter main reflector, while refurbishment of the telescope was completed in 2015 resulting in enlargement of the main reflector of 26 m and improvement of the antenna surface accuracy. Receivers at five frequency bands, L, S/X, C, K, and Q, are equipped, while the new Q-band cooled receiver had been installed in 2018 and now is under evaluation. The surface accuracy of main- and sub-reflectors are 0.4 mm rms and 0.1 mm rms, respectively. The slewing rates of the main reflector are 1.0°/sec in azimuth and 0.5°/sec in elevation, as shown in Table 3.

Table 3: Driving performance of EAVN telescopes.

rable of Briting performance of Erryr, telegoopes.							
Driving range	Max. driving speed	Max. driving acceleration					
	Nobeyama						
$-60^{\circ} \sim 510^{\circ}$	$0.3^{\circ}/\mathrm{sec}$	$0.3^{\circ}/\mathrm{sec}^2$					
$12^{\circ} \sim 80^{\circ}$	$0.3^{\circ}/\mathrm{sec}$	$0.3^{\circ}/\mathrm{sec^2}$					
	Takahagi	·					
$11^{\circ} \sim 349^{\circ}$	$0.07^{\circ}/\mathrm{sec}$	$0.035^{\circ}/{\rm sec^2}$					
$15^{\circ} \sim 70^{\circ}$	$0.07^{\circ}/\mathrm{sec}$	$0.035^{\circ}/\mathrm{sec}^2$					
	Tianma	·					
$-60^{\circ} \sim 425^{\circ}$	$0.5^{\circ}/\mathrm{sec}$	$0.27^{\circ}/\mathrm{sec}^2$					
$8^{\circ} \sim 88^{\circ}$	$0.3^{\circ}/\mathrm{sec}$	$0.16^{\circ}/\mathrm{sec^2}$					
	Nanshan						
$-270^{\circ} \sim 270^{\circ}$	$1.0^{\circ}/\mathrm{sec}$	$0.5^{\circ}/\mathrm{sec^2}$					
$5^{\circ} \sim 88^{\circ}$	$0.5^{\circ}/\mathrm{sec}$	$0.5^{\circ}/\mathrm{sec^2}$					
VERA							
$-90^{\circ} \sim 450^{\circ}$	$2.1^{\circ}/\mathrm{sec}$	$2.1^{\circ}/\mathrm{sec}^2$					
$5^{\circ} \sim 85^{\circ}$	$2.1^{\circ}/\mathrm{sec}$	$2.1^{\circ}/\mathrm{sec^2}$					
$-270^{\circ} \sim 270^{\circ}$	$3.1^{\circ}/\mathrm{sec}$	$3.1^{\circ}/\mathrm{sec^2}$					
	KVN						
$-90^{\circ} \sim 450^{\circ}$	$3.0^{\circ}/\mathrm{sec}$	$3.0^{\circ}/\mathrm{sec}^2$					
$5^{\circ} \sim 85^{\circ}$	$3.0^{\circ}/\mathrm{sec}$	$3.0^{\circ}/\mathrm{sec^2}$					
	Driving range $-60^{\circ} \sim 510^{\circ} \\ 12^{\circ} \sim 80^{\circ}$ $11^{\circ} \sim 349^{\circ} \\ 15^{\circ} \sim 70^{\circ}$ $-60^{\circ} \sim 425^{\circ} \\ 8^{\circ} \sim 88^{\circ}$ $-270^{\circ} \sim 270^{\circ} \\ 5^{\circ} \sim 85^{\circ} \\ -270^{\circ} \sim 270^{\circ}$ $-90^{\circ} \sim 450^{\circ}$ $-90^{\circ} \sim 450^{\circ}$						

^aThe north is 0° and the east is 90° .

Table 4: Aperture efficiency and beam size of EAVN telescopes.

	K-band (22 GHz)		Q-ban	d (43 GHz)
	$\overline{\eta_{ m A}}$	HPBW	$\overline{\eta_{ m A}}$	HPBW
Telescope name	(%)	(arcsec)	(%)	(arcsec)
Nobeyama	61	72	53	39
Takahagi	30	100	_	_
Tianma	50	44	45	22
Nanshan	60	115	_	_
Mizusawa	48	139	50	74
Iriki	44	147	40	74
Ogasawara	43	142	42	74
Ishigakijima	44	142	42	72
Yonsei	55	127	63	63
Ulsan	63	124	61	63
Tamna	60	126	63	63

^bField rotator. FR is 0° when Beam-1 is at the sky side and Beam-2 is at the ground side, and CW is positive when a telescope is seen from a target source.

2.2.7 Aperture Efficiency

The aperture efficiency of each VERA antenna is about 40–50% in both K- and Q-bands (see Table 4 for the 2019-2020 and 2012 data for VERA and KVN, respectively). The latest values for VERA were measured in 2018 December-March and 2020 February-March. These measurements were based on the observations of Jupiter assuming that the brightness temperature of Jupiter is 160 K in both K- and Q-bands. Due to the bad weather condition in some of the sessions, the measured efficiencies show large scatter. However, we conclude that the aperture efficiencies are not significantly changed compared with previous measurements. The elevation dependence of aperture efficiency for VERA antenna was also measured from the observation toward maser sources. Figure 4 shows the relations between the elevation and the aperture efficiency measured for VERA Iriki station. The gain curves are measured by observing the total power spectra of intense maser sources. The aperture efficiency in low elevation of ≤ 20 deg decreases slightly, but this decrease is less than about 10%. Concerning this elevation dependence, the observing data FITS file include a gain curve table (GC table), which is AIPS readable, in order to calibrate the dependence when the data reduction.

The aperture efficiency and beam size for each KVN antenna are also listed in Table 4. Aperture efficiency of KVN varies with elevation as shown in Figure 4. The main reflector panels of KVN antennas were installed to give the maximum gain at the elevation angle of 48°. The sagging of sub-reflector and the deformation of main reflector by gravity with elevation results in degradation of antenna aperture efficiency with elevation. In order to compensate this effect, KVN antennas use a hexapod to adjust sub-reflector position. Figure 4 shows the elevation dependence of antenna aperture efficiency of the KVN 21 m radio telescopes measured by observing Venus or Jupiter. By fitting a second order polynomial to the data and normalizing the fitted function with its maximum, we derived a normalized gain curve which has the following form:

$$G_{\text{norm}} = A_0 E L^2 + A_1 E L + A_2,$$
 (1)

where EL is the elevation in degree.

Aperture efficiency and beam size for non-KaVA telescopes are also summarized in Table 4. The values for NRO45 are based on the latest measurements in autumn 2017, where the Jupiter or the Mars was used as a reference source. The elevation dependence of the aperture efficiency is approximately constant over a range of El $\sim 25^{\circ}$ – 50° at both K- and Q-bands.

The aperture efficiency of TMRT65 is above 45% at both K- and Q-bands with the active surface control system. The main reflector panels were assembled to give the maximum surface accuracy at the elevation angle of 52°. The aperture efficiency goes down to less than 10% at low (< 10°) and high (> 80°) elevation angles, mainly due to the gravitational deformation. The active surface control system is used for compensating the gravitational effect at different elevation angles, making the gain curves as a constant over the elevation. Figure 5 shows the elevation dependence of the aperture efficiency at Q-band with or without the active surface control. The active surface control system is set 'ON' by default at K- and Q-band observations.

The aperture efficiency of TAK32 and NSRT26 is 30% and 60% at K-band, respectively.

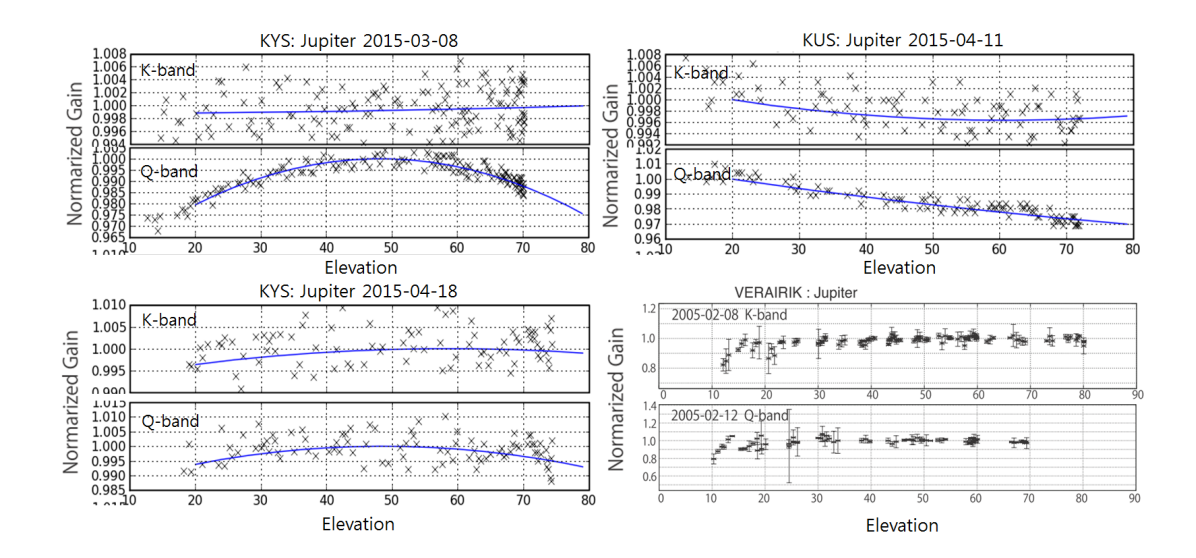


Figure 4: The elevation dependence of the aperture efficiency for KVN three antennas and VERA Iriki antenna. For KVN antennas, the maximum gain is given at the elevation angle of 48° . The efficiency in K-band (on Feb 8, 2005) and the Q-band (on Feb 12, 2005) for VERA Iriki antenna is shown in *bottom right*. The efficiency is relative value to the measurement at EL = 50° .

2.2.8 Beam Pattern and Size

Figure 6 shows the beam patterns for VERA at K-band. The side-lobe level is less than about $-15 \, \mathrm{dB}$, except for the relatively high side-lobe level of about $-10 \, \mathrm{dB}$ for the separation angle of 2.0 deg at Ogasawara station. The side-lobe of the beam patterns has an asymmetric shape, but the main beam has a symmetric Gaussian shape without dependence on separation angle. The measured beam sizes (HPBW) in K- and Q-bands based on the data of the pointing calibration are also summarized in Table 4. The main beam sizes show no dependence on the dual-beam separation angle.

The optics of KVN antenna is a shaped Cassegrain type of which the main reflector and subreflector are shaped to have a uniform illumination pattern on an aperture plane. Because of the uniform illumination, KVN antennas can get higher aperture efficiency than value of typical Cassegrain type antenna. However, higher side-lobe level is inevitable. OTF images of Jupiter at K- and Q-bands are shown in Figure 6. The map size is 12'×10' and the first side-lobe pattern is clearly visible. Typical side-lobe levels of KVN antennas are 13-14dB.

2.3 Receivers

2.3.1 Brief Summary of VERA Receiving System

Each VERA antenna has the receivers for 4 bands, which are S (2 GHz), C (6.7 GHz), X (8 GHz), K (22 GHz), and Q (43 GHz) bands. For the open use, K-band and Q-band are open for observation. The low-noise HEMT amplifiers in the K- and Q-bands are enclosed in the cryogenic dewar, which is cooled down to 20 K, to reduce the thermal noise. The range of observable frequency and the typical receiver noise temperature

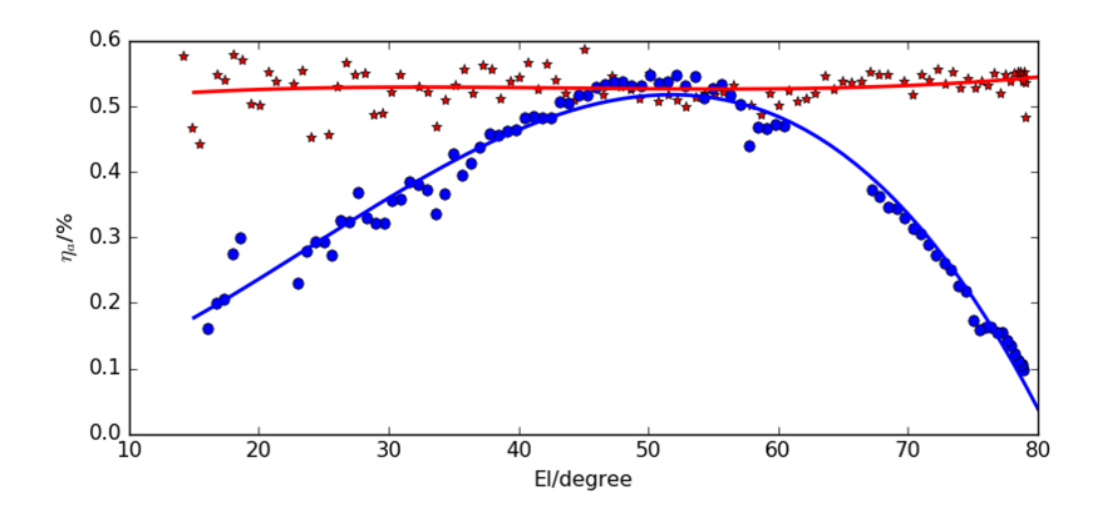


Figure 5: Elevation dependence of the aperture efficiency (η_{eff}) for TMRT65 at Q-band. The red and blue colors represent η_{eff} with or without the active surface control, respectively.

 $(T_{\rm RX})$ at each band are summarized in Table 5 and Figure 7.

After the radio frequency (RF) signals from astronomical objects are amplified by the receivers, the RF signals are mixed with standard frequency signal generated in the first local oscillator to down-convert the RF to an intermediate frequency (IF) of 4.7 GHz – 7 GHz. The first local frequencies are fixed at 16.8 GHz in K-band and at 37.5 GHz in Q-band. The IF signals are then mixed down again to the base band frequency of 0 – 512 MHz. The frequency of second local oscillator is tunable with a possible frequency range between 4 GHz and 7 GHz. The correction of the Doppler effect due to the earth rotation is carried out in the correlation process after the observation. Therefore, basically the second local oscillator frequency is kept to be constant during the observation. Figure 8 shows a flow diagram of these signals for VERA.

2.3.2 Brief Summary of KVN Receiving System

The KVN quasi-optics are uniquely designed to observe 22, 43, 86 and 129 GHz band simultaneously [4], [5]. Figure 9 shows the layout of quasi-optics and receivers viewing from sub-reflector side. The quasi-optics system splits one signal from sub-reflector into four using three dichroic low-pass filters marked as LPF1, LPF2 and LPF3 in the Figure 9. The split signals into four different frequency bands are guided to corresponding receivers.

Figure 10 shows a signal flows in KVN system. The 22, 43 and 86 GHz band receivers are cooled HEMT receivers and the 129 GHz band receiver is a SIS mixer receiver. All receivers can receive dual-circular-polarization signals. Among eight signals (four dual-polarization signals), four signals selected by the IF selector are down-converted to the input frequency band of the sampler. The instantaneous bandwidth of the 1st IF of each receiver is limited to 2 GHz by the band-pass filter. The 1st IF signal is down-converted by BBCs to the sampler input frequency (512-1024 MHz) band.

Typical noise temperatures of K- and Q-bands are presented in Table 5. Since the

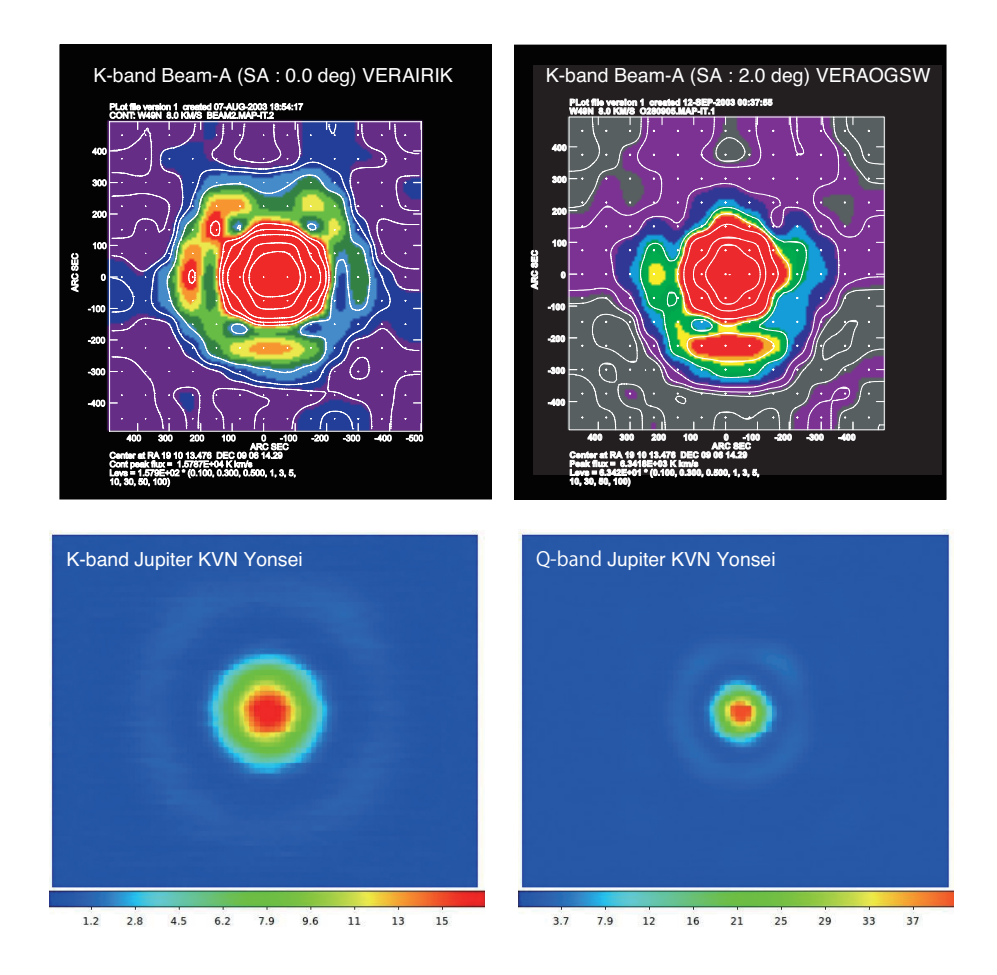


Figure 6: The beam patterns in the K-band for VERA (A-beam) Iriki with the separation angle of 0° (*Upper left*) and Ogasawara with the separation angle of 2.0° (*Upper right*), and in K/Q-band for KVN Yonsei. The patterns of VERA antennas were derived from the mapping observation of strong H₂O maser toward W49N, which can be assumed as a point source, with grid spacing of 75". In the case of KVN antennas, the patterns were derived from the OTF images of Venus at K/Q-band.

calibration chopper is located before the quasi-optics as shown in Figure 9, the loss of quasi-optics contributes to receiver noise temperature instead of degrading antenna aperture efficiency. Therefore, the noise temperature in the table includes the contribution due to the quasi-optics losses.

2.3.3 Brief Summary of NRO45 Receiving System

The NRO45 covers an observing frequency range of 20-116 GHz with multiple receivers. The VLBI backend system of the NRO45 is currently equipped at K-band and Q-band. Figure 11 illustrates a flow diagram of the VLBI receiving system in the NRO45. The observable RF range and typical receiver noise temperature for the receivers at K- and Q-bands are also summarized in Table 5. The received RF signals are down-converted into an IF range of 5-7 GHz, and the IF signals are then mixed down to the base band of 512-1024 MHz, which is the input to the A/D sampler.

Currently, one of the receivers can be selected by switching the mirrors in the optics in a few minutes manually. In the near future, K- and Q-band observations can be

Table 5: Fre	quency range an	$d T_{PY}$ of	receivers at	each EAVN	telescope.
Table 9. III	quelle y lange an	$u \perp R \chi \cup I$	I C C C I V C I D C U		UCICOCOPC.

Band	Frequency Range	$T_{\mathrm{RX}}{}^{a}$	Polarization						
	[GHz]	[K]							
	Nobeyama								
K	21.5 - 23.8	~ 85	LCP/RCP						
Q	42.5 - 44.5	~ 111	LCP						
		Takahagi							
K	21.0 - 25.0	~ 30	LCP/RCP						
		Tianma							
K	18.0 - 26.5	16 - 35	LCP/RCP						
Q	39 - 47	35 - 50	LCP/RCP						
	Nanshan								
K	22.0 - 24.2	~ 15	LCP/RCP						
Q	(1	under evaluation)							
		VERA							
K	21.5 - 23.8	30 - 50	LCP						
Q	42.5 - 44.5	70 - 90	LCP						
KVN									
K	18 - 26	20 - 40	LCP/RCP						
Q	35 - 50	40 - 50 (Yonsei)	LCP/RCP						
	42.11 - 44.11	40 - 50 (Ulsan)	LCP/RCP						
	42.11 - 44.11	70 - 80 (Tamna)	LCP/RCP						
aD acci	ron noice temperati								

^aReceiver noise temperature

conducted simultaneously by inserting a perforated high-pass dichroic plate. When using the dichroic plate, the gain of the Q-band signals may be reduced by 0.3dB (in 2018 June), causing the rise of the system noise temperature by about 30 K.

2.3.4 Brief Summary of TAK32 Receiving System

Figure 12 shows a flow diagram of the VLBI receiving system in TAK32. TAK32 covers an observing frequency range of 6-9 GHz and 21-25 GHz with two criogenically-cooled receivers, while TAK32 joins in EAVN observations at only K-band in the 2020B semester.

The flow diagram of TAK32 is shown in Figure 12. The K-band receiver is cooled with dual circular polarization. The observable frequency range and the typical receiver noise temperature are shown in Table 5. The total system noise temperatures at K-band is typically 40 K at winter with good weather, > 100 K at winter with bad weather, 150 K at summer with good weather, and > 500 K at summer with bad weather.

For K-band, received RF signals are down-converted into an IF range of 8.0-8.8 GHz, and the IF signals are then mixed down to the base band of 512-1024 MHz, which is the input to the A/D sampler ADS-3000+. The data with the rate of 1024 MHz \times 2 bit are recorded by OCTADISK, and then the digital base-band converter is used to convert the 2 Gbps data into 1 Gbps.

2.3.5 Brief Summary of TMRT65 Receiving System

Figure 13 shows a flow diagram of the VLBI receiving system in TMRT65. TMRT65 has the receivers for 8 frequency bands, L (1.4 GHz), S/X (2.3/8.4 GHz), C (6.7 GHz),

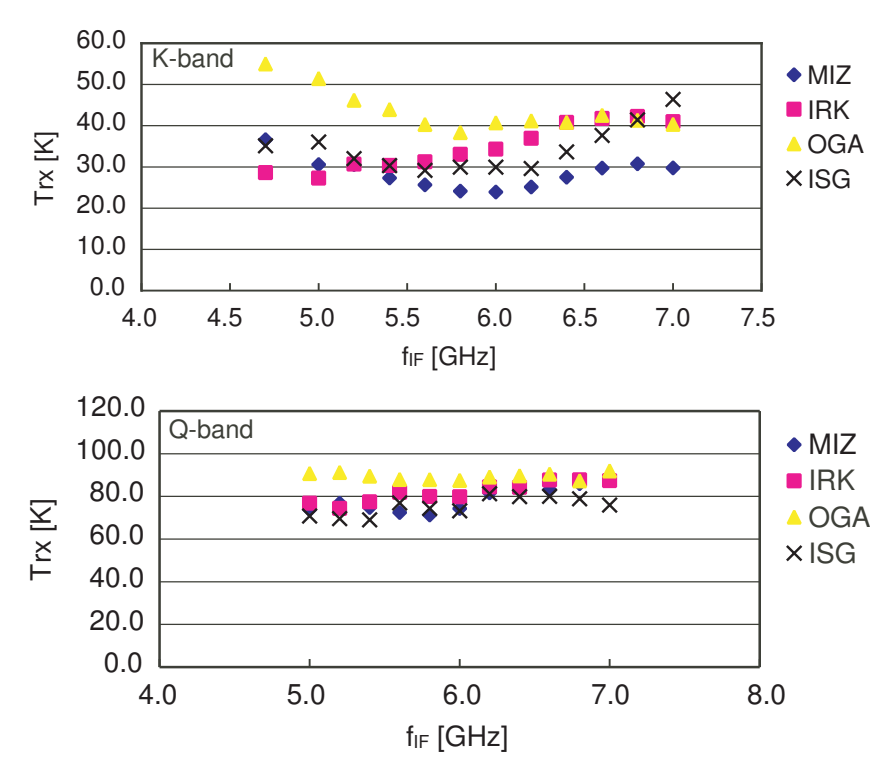


Figure 7: Receiver noise temperature for each VERA antenna. Top and bottom panels show measurements in the K- and Q-bands, respectively. Horizontal axis indicate an IF (intermediate frequency) at which $T_{\rm RX}$ is measured. To convert it to RF (radio frequency), add 16.8 GHz in K-band and 37.5 GHz in Q-band to the IF frequency.

X/Ka (8.4/31.0 GHz), Ku (15 GHz), K (22 GHz), and Q (43 GHz). The K- and Q-band receivers are cooled HEMT receivers with dual circular polarizers. The observable frequency range and the typical receiver noise temperature are shown in Table 5. The total system noise temperatures at K- and Q-bands are typically 70 and 110 K, respectively. The RF signal is firstly down-converted to IF range of 4-12 GHz and it is transferred by optical fibers to the observing room, where the signal is further down-converted to 0-1024 MHz (actually in 10-512 MHz and 512-1024 MHz) at the input of BBCs.

2.3.6 Brief Summary of NSRT26 Receiving System

Figure 14 shows a flow diagram of the VLBI receiving system in NSRT26. NSRT26 has the receivers for 5 frequency bands, L (1.4 GHz), S/X (2.3/8.4 GHz), C (5 GHz), K (22 GHz), and Q (43 GHz), while NSRT26 joins in EAVN observations at only K-band in the 2020B semester. The K-band receiver is cooled HEMT receivers with dual circular polarizers. The observable frequency range and the typical receiver noise temperature are shown in Table 5. The total system noise temperatures at K-band is typically 42 K. The RF signal is down-converted with three stages, and analog-digital conversion and digital filtering of the IF signal is conducted using either the Digital Baseband Converter (DBBC) system or the Chinese VLBI Data Acquisition System (CDAS).

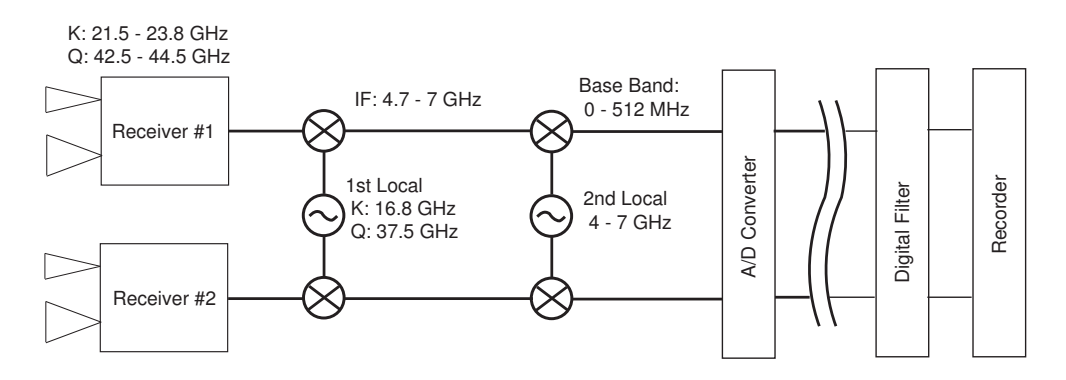


Figure 8: Flow diagram of signals from receiver to recorder for VERA.

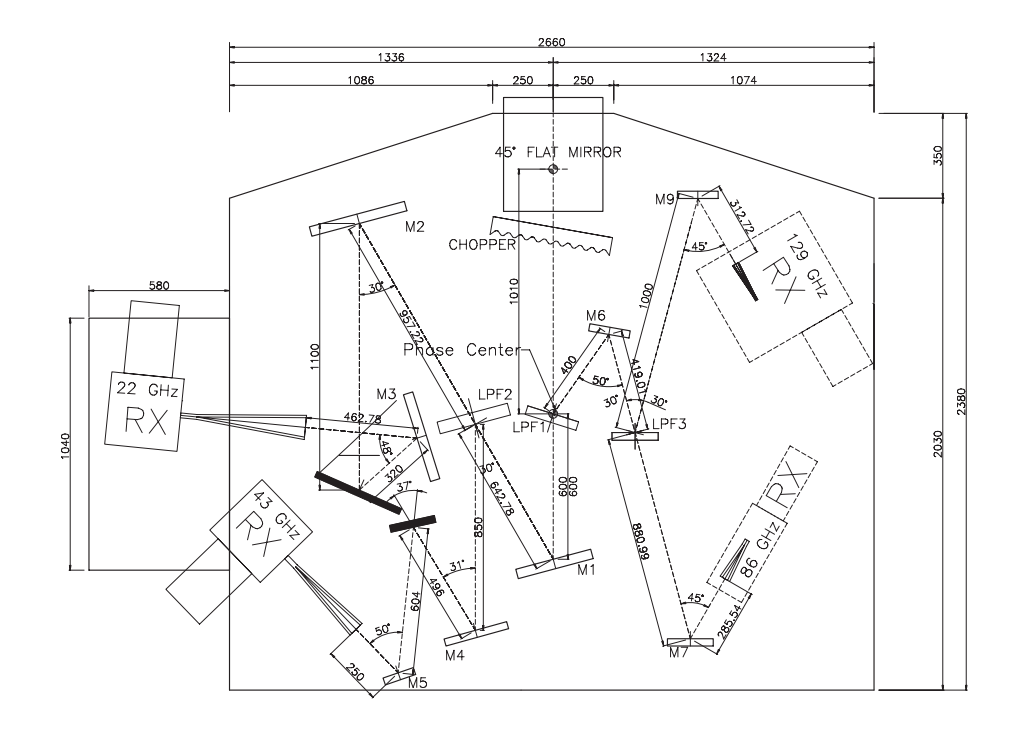


Figure 9: KVN multi-frequency receiving system [4], [5].

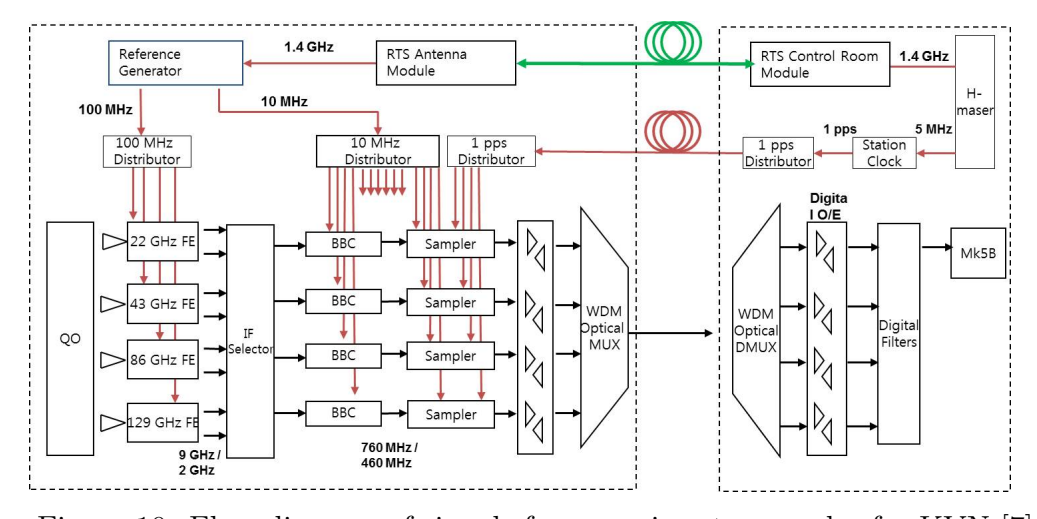


Figure 10: Flow diagram of signals from receiver to recorder for KVN [7].

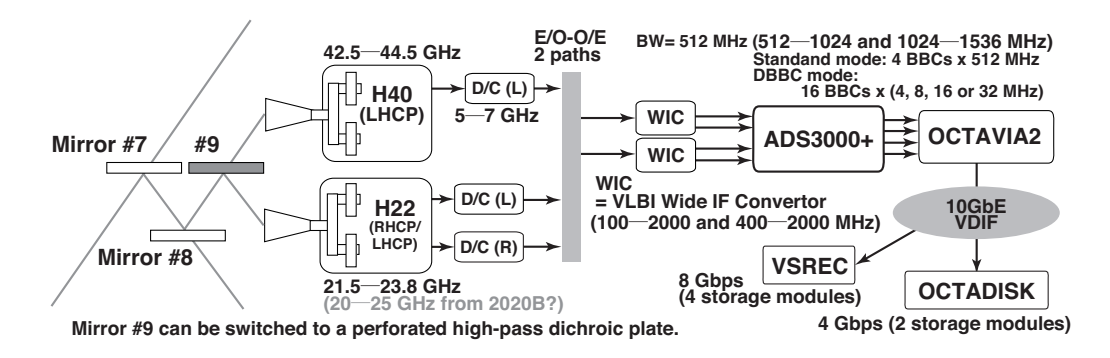


Figure 11: Flow diagram of signals from receiver to recorder for NRO45.

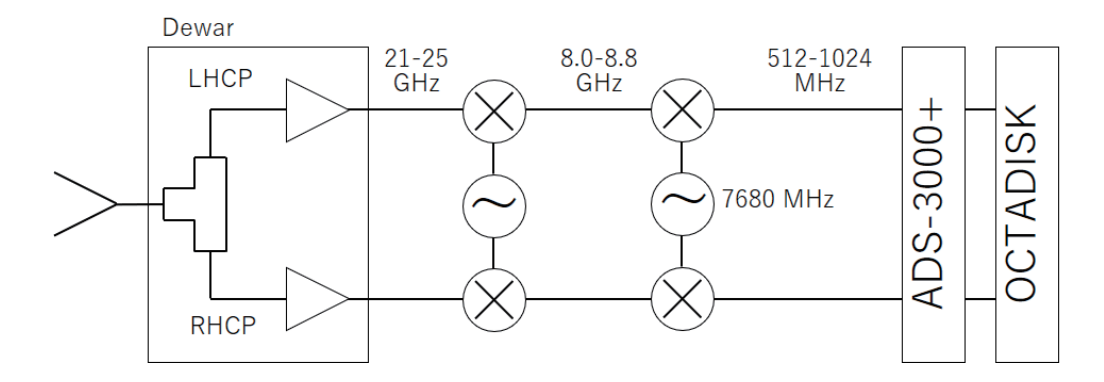


Figure 12: Flow diagram of signals from receiver to recorder for TAK32.

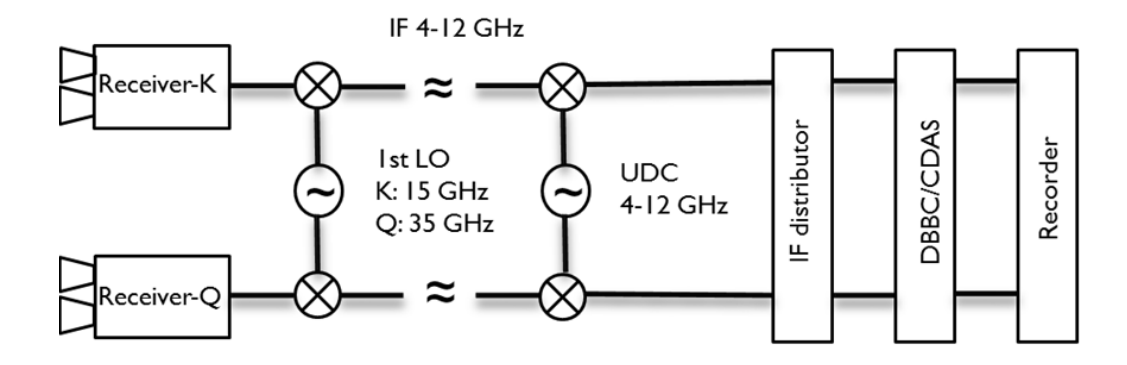


Figure 13: Flow diagram of signals from receiver to recorder for TMRT65.

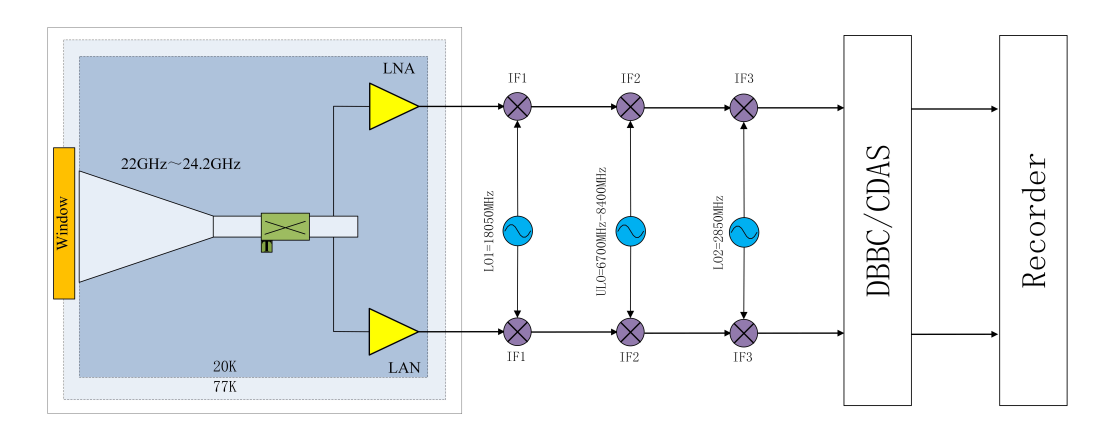


Figure 14: Flow diagram of signals from receiver to recorder for NSRT26.

2.4 Digital Signal Processing

In VERA system, A/D (analog-digital) samplers convert the analog base band outputs of 0-512 MHz \times 2 beams to digital form. The A/D converters carry out the digitization of 2-bit sampling with the bandwidth of 512 MHz and the data rate is 2048 Mbps for each beam.

In KVN system, A/D samplers digitize signals into 2-bit data streams with four quantization levels. The base band output is 512 - 1024 MHz. The sampling rate is 1024 Mega sample per second (Msps) with 2-bit sampling, resulting in the data rate of 2 Gbps at the frequency bandwidth of 512 MHz. Four streams of 512 MHz band width (2 Gbps data rate) can be obtained in the KVN multi-frequency receiving system simultaneously, which means that the total rate is 8 Gbps.

In NRO45 system, the baseband signal output is 512 - 1024 MHz and the A/D samplers perform 2-bit digitization with four quantization levels. A maximum recording rate of 2048 Mbps is possible with a total bandwidth of 512 MHz.

Since the total data recording rate is limited to 1024 Mbps (see the next section), only part of the sampled data can be recorded onto hard disks. The data rate reduction is done by digital filter system, with which one can flexibly choose number and width of recording frequency bands.

Observers can select modes of the digital filter listed in the Table 6. In VERA7SIOS mode in the Table 6, two transitions (v=1 & 2) of SiO maser in the Q band can be simultaneously recorded.

2.5 Recorders

The EAVN observations are basically limited to record with 1024 Mbps data rate. To response 1 Gbps recording, VERA, NRO45, and TAK32 have OCTADISK. KVN, TMRT65, and NSRT26 use the Mark5B recording systems. OCTADISK and Mark5B are hard disk recording systems developed at NAOJ and Haystack observatory, respectively. The total bandwidth is 256 MHz.

2.6 Correlators

The correlation process is carried out by a VLBI correlator located at KJCC (Korea-Japan Correlation Center) at Daejeon, which has been developed as the KJJVC (Korea-Japan Joint VLBI Correlator) located at KJCC (Korea-Japan Correlation Center) project. Hereafter it is tentatively called "Daejeon correlator". Specification of The Daejeon correlator is summarized in Table 8. The Daejeon correlator can process the data stream of up to 8192 Mbps from maximum 16 antenna stations at once. Currently the raw observed data of KVN, TMRT65, and NSRT26 stations are recorded and playbacked with Mark5B, and those of VERA, NRO45, and TAK32 are recorded and playbacked with OCTADISK at the data rate of 1024 Mbps. For KaVA, data formats available in the next observing season are 16 IFs \times 16 MHz ("C5 mode" in The Daejeon correlator terminology), 8 IFs \times 32 MHz (C4 mode), and 2 IFs \times 128 MHz (C2 mode). For EAVN (including non-KaVA telescopes), available data formats are 16 IFs \times 16 MHz (C5 mode) at K-band, and 8 IFs \times 32 MHz (C4 mode) at both K-and Q-bands. Note that the C2 mode is available at only KaVA 7 telescopes. Minimum

Table 6: Digital filter mode for EAVN.

Mode	Rate	Num.	$\mathrm{BW}/\mathrm{CH}^b$		Freq. range ^{d}	Side	
Name	(Mbps)	CH^a	(MHz)	CH^c	(MHz)	Band^e	Note^f
GEO1K*	1024	16	16	1	0 - 16	U	
				2	32 - 48	U	
				3	64 - 80	U	
				4	96 - 112	U	
				5	128 - 144	U	
				6	160 - 176	U	
				7	192 - 208	U	
				8	224 - 240	U	
				9	256 - 272	U	Target line (e.g. H_2O)
				10	288 - 304	U	
				11	320 - 336	U	
				12	352 - 368	U	
				13	384 - 400	U	
				14	416 - 432	U	
				15	448 - 464	U	
				16	480 - 496	U	
GEO1S*	1024	16	16	1	112 - 128	L	
				2	128 - 144	U	
				3	144 - 160	${ m L}$	
				4	160 - 176	U	
				5	176 - 192	${ m L}$	
				6	192 - 208	U	
				7	208 - 224	${ m L}$	
				8	224 - 240	U	
				9	240 - 256	${ m L}$	
				10	256 - 272	U	Target line (e.g. H_2O)
				11	272 - 288	${ m L}$	
				12	288 - 304	U	
				13	304 - 320	${ m L}$	
				14	320 - 336	U	
				15	336 - 352	${ m L}$	
				16	352 - 368	U	
VERA7SIOS*	1024	16	16	1	32 - 48	U	
				2	64 - 80	U	
				3	80 - 96	L	SiO $(J=1-0, v=2)$
				4	96 - 112	U	
				5	128 - 144	U	
				6	160 - 176	U	
				7	192 - 208	U	
				8	224 - 240	U	
				9	256 - 272	U	
				10	288 - 304	U	
				11	384 - 400	U	SiO $(J=1-0, v=1)$
				12	320 - 336	U	, , ,
				13	352 - 368	U	
				14	416 - 432	Ü	
				15	448 - 464	Ü	
				16	480 - 496	Ü	
* All channels a	ro for A B	Ponm (VI	FRA) and I		ERA/KVN). Mo		os aro tontativo

^{*}All channels are for A-Beam (VERA) and LCP (VERA/KVN). Mode names are tentative. $^a\mathrm{Total}$ number of channels

 $[^]b\mathrm{Bandwidth}$ per channel in MHz

^cChannel number

 $[^]d\mathrm{Filtered}$ frequency range in the base band (MHz) $^e\mathrm{Side}$ Band (LSB/USB)

fExample of spectral line setting

integration times (time resolution) are 0.2048, 0.8192, and 1.6384 seconds for C2, C4, and C5 modes, respectively, and the number of frequency channels within each IF is 8192 for both modes (i.e. maximum frequency resolution is about 1.95 kHz). By default, the number of frequency channels is reduced to 128 (for continuum) or 512 (for line) via channel integration after correlation. One may put a special request of number of frequency channels to take better frequency resolution. The number of frequency channels can be selected among 512, 1024, 2048, 4096 or 8192. Final correlated data is served as FITS-IDI file.

2.6.1 Note for the C2 mode

To obtain the accurate amplitude values across the all IF channels, however, it is better to reduce the number of baseband (or IFs in data handling with AIPS) yielded by the digital filter unit (DFU) so that the amplitude losses at the edge of each baseband are avoided. This reduction is especially helpful to observe continuum sources, such as active galactic nuclei (AGN). For this purpose, C2 mode, which has 2 IFs \times 128 MHz, is opened for EAVN although the mode can be employed for an observation with only KaVA 7 telescopes.

When using the C2 mode, note the following two matters: (i) There is a moderate amplitude slope in an IF channel mainly at VERA stations, which must be corrected by all the gain calibration procedures in AIPS (AIPS tasks ACCOR, BPASS, and APCAL): (ii) KaVA's observation data is conventionally correlated by the Daejeon Hardware Correlator. In this case, the scaling factor of 1.3 should be applied to the data to recover the quantization loss ¹ [6].

2.7 Calibration

Here we briefly summarize the calibration procedure of the EAVN data. Basically, most of the post-processing calibrations are done by using the AIPS (Astronomical Image Processing System) software package developed by NRAO (National Radio Astronomical Observatory).

2.7.1 Delay and Bandpass Calibration

The time synchronization for each antenna is kept within 0.1 μ sec using GPS and high stability frequency standard provided by the hydrogen maser. To correct for clock parameter offsets with better accuracy, bright continuum sources with accurately-known positions should be observed at usually every 60-80 minutes during observations. A recommended scan length for calibrators is 5-10 minutes. This can be done by the AIPS task FRING. The calibration of frequency characteristic (bandpass calibration) can be also done based on the observation of bright continuum source. This can be done by the AIPS task BPASS.

¹This scaling factor is conventionally applied to the data using the AIPS task APCAL, however this is not applicable if the data is loaded to AIPS using the AIPS task FITLD with DIGICOR = 3.

2.7.2 Gain Calibration

VERA, KVN, NRO45, and TAK32 antennas have the chopper wheel of the hot load (black body at the room temperature), and the system noise temperature can be obtained by measuring the ratio of the sky power to the hot load power (so-called R-Sky method). Thus, the measured system noise temperature is a sum of the receiver noise temperature, spillover temperature, and contribution of the atmosphere (i.e. so-called $T_{\rm sys}^*$ corrected for atmospheric opacity). The hot load measurement can be made before/after any scan at all telescopes except TAK32. TAK32 measures the system noise temperature at the timing of when the telescope operator decides the measurement before or after any scan. Also, the sky power is continuously monitored during scans, so that one can trace the variation of the system noise temperature. The system noise temperature value can be converted to SEFD (System Equivalent Flux Density) by dividing by the antenna gain in K/Jy, which is derived from the aperture efficiency and diameter of each antenna.

For the correlated data from KJCC, $T_{\rm sys}^*$ data (TY table) and antenna gain information (GC table) are provided with the ANTAB-readable format. KJCC makes complete version of ANTAB-readable file and provide it to PI. User support team supports PIs as appropriate. The TY and GC tables can be loaded by the AIPS task ANTAB, and these tables are converted to the SN table by the AIPS task APCAL.

On the other hand, $T_{\rm sys}$ measurement provided by TMRT65 and NSRT26 contains atmospheric opacity effects, thus the opacity correction should be applied to those data in the course of data reduction.

Alternatively, one can calibrate the visibility amplitude by the template spectrum method, in which auto-correlation spectra of a maser source is used as the flux calibrator. This calibration procedure is made by the AIPS task ACFIT (see AIPS HELP for ACFIT and Cho et al. (2017) [3] for more details). For an EAVN observation including TMRT65, NRO45, TAK32, and NSRT26, we strongly recommend users to observe a maser source or a compact continuum gain calibrator for every ≤ 1 hr. This offers an additional cross-check of the amplitude calibration for TMRT65/NRO45. Along with this, these two telescopes will do regular antenna pointing scans for every $\leq 1-2$ hr.

As for TMRT65, moreover, frequent pointing check is necessary for observations at both K- and Q-bands. The pointing check is done semi-automatically with a continuum back-end system and the quality of pointing check is judged by on-site operators. We strongly recommend to keep at least 3 minutes for the pointing check itself with additional slewing time between target and pointing sources. For example, it is preferable to secure 5-min gap in total for the pointing check toward a pointing source with the angular separation of $\sim 15^{\circ}$ from the target.

Further correction is made for VLBI observations taken with 2-bit (4-level) sampling, for the systematic effects of non-optimal setting of the quantizer voltage thresholds. This is done by the AIPS task ACCOR. Another correction should be applied to recover the amplitude loss, which are attributed to the combination of two steps of 2-bit quantization in the digital filtering at the backend system and characteristics of Daejeon correlator. This is done by multiplying the scaling factor of 1.3 (the best current estimation) [6] in the AIPS task APCAL (adverbs APARM(1) = 1.3, OPCODE = ", and DOFIT = 1) or SNCOR (adverbs OPCODE = "MULA", and SNCORPRM(1) = 1.3). Note that this correction should be applied to all EAVN telescopes. The amplitude

2.8 Geodetic Measurement

2.8.1 Brief Summary of VERA Geodetic Measurement

Geodetic observations are performed as part of the VERA project observations to derive accurate antenna coordinates. The geodetic VLBI observations for VERA are carried out in the S/X-bands and also in the K-band. The S/X-bands are used in the domestic experiments with the Geographical Survey Institute of Japan and the international experiments called IVS-T2. On the other hand, the K-band is used in the VERA internal experiments. We obtain higher accuracy results in the K-band compared with the S/X-bands. The most up-to-date geodetic parameters are derived through geodetic analyses.

Non-linear post seismic movement of Mizusawa after the 2011 off the Pacific coast of Tohoku Earthquake continues. The position and velocity of Mizusawa is continuously monitored by GPS. The coordinates in Table 1 are provisional and will be revised with accumulation of geodetic data by GPS and VLBI.

In order to maintain the antenna position accuracy, the VERA project has three kinds of geodetic observations. The first is participation in JADE (JApanese Dynamic Earth observation by VLBI) organized by GSI (Geographical Survey Institute) and IVS-T2 session in order to link the VERA coordinates to the ITRF2008 (International Terrestrial Reference Frame 2008). Basically Mizusawa station participates in JADE nearly every month. Based on the observations for four years, the three-dimensional positions and velocities of Mizusawa station till 2011 March 9 is determined with accuracies of 7 – 9 mm and about 1 mm/yr in ITRF2008 coordinate system. But the uncertainty of several centimeters exists in the position on and after 2011 March 11. The second kind of geodetic observations is monitoring of baseline vectors between VERA stations by internal geodetic VLBI observations. Geodetic positions of VERA antennas relative to Mizusawa antenna are measured from geodetic VLBI observations every two weeks. From polygonal fitting of the six-year geodetic results, the relative positions and velocities are obtained at the precisions of 1-2 mm and 0.8-1 mm/yr till 2011 March 10. The third kind is continuous GPS observations at the VERA sites for interpolating VLBI geodetic positions. Daily positions can be determined from 24 hour GPS data. The GPS observations are also used to estimate tropospheric zenith delay of each VERA site routinely. The time resolution of delay estimates is 5 minutes.

2.8.2 Brief Summary of KVN Geodetic Measurement

KVN antenna positions are regularly monitored using GPS and geodetic VLBI observations. The K-band geodesy VLBI program between KVN and VERA has been started in 2011. Current KVN antenna positions (see Figure 15) are obtained from the KaVA K-band geodesy on 2014 January 24. The typical 1-sigma errors of geodetic solutions are about 0.4 cm in X, Y, and Z directions. Based on 22-epoch KaVA K-band geodetic observations from September 2012 to December 2016, uncertainty of KVN antenna positions are ~ 2.38 cm at Yonsei, ~ 2.55 cm at Ulsan and ~ 1.58 cm at Tamna.

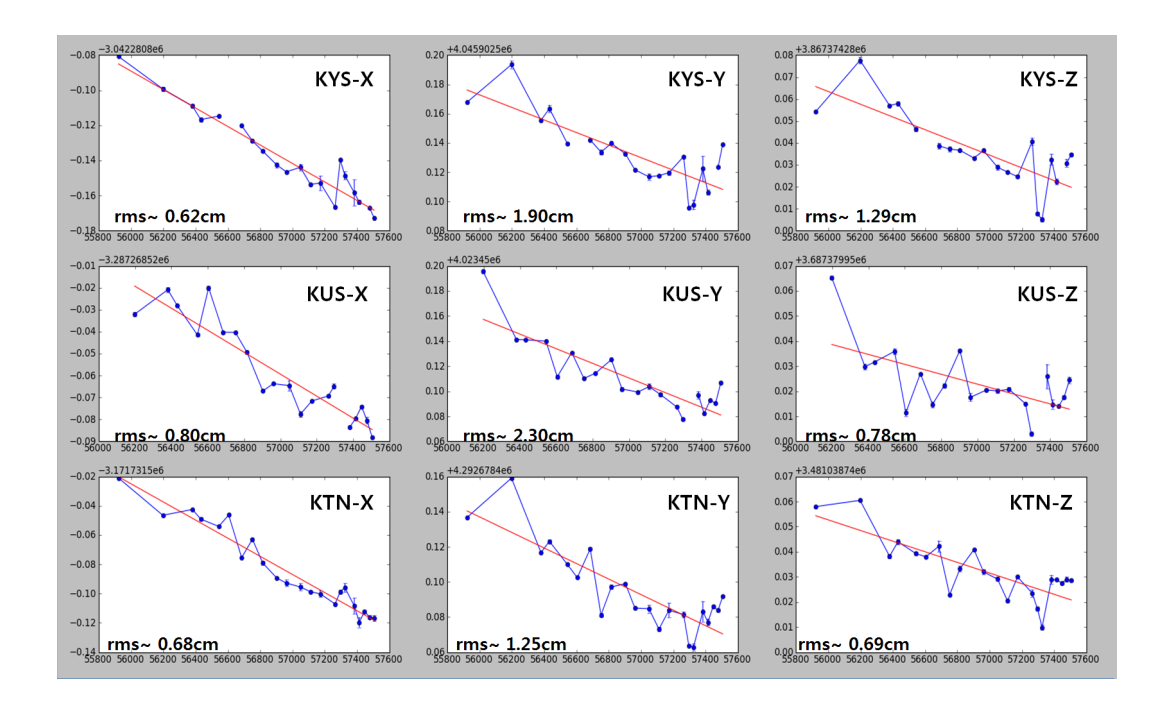


Figure 15: The trend of KVN antenna positions (IVP) in ITRF2014 coordinate system. The x and y axes are MJD and $\rm X/Y/Z$ in meter. The linear fitted is applied to the measurements, shown as red line, and its deviation is also presented in each axis as "rms".

Table 7: Digital filter mode for EAVN — continued.

Mode	Rate	Num.	BW/CH^b		Freq. range d	Side	
Name	(Mbps)	CH^a	(MHz)	CH^c	(MHz)	Band^e	$Note^f$
VERA4S*	1024	8	32	1	128 - 160	U	
				2	160 - 192	L	
				3	192 - 224	U	
				4	224 - 256	L	
				5	256 - 288	U	
				6	288 - 320	L	
				7	320 - 352	U	
				8	352 - 384	L	
VERA1S*	1024	2	128	1	128 - 256	L	
				2	256 - 384	U	

^{*}All channels are for A-Beam (VERA) and LCP (VERA/KVN).

 $[^]a$ Total number of channels

^bBandwidth per channel in MHz

^cChannel number

^dFiltered frequency range in the base band (MHz)

^eSide Band (LSB/USB)

Table 8: Specification of The Daejeon $correlator^a$.

	<u> </u>
Max. number of antennas	16
correlation mode	$C2^b$ (128 MHz Bandwidth, 2 stream)
	C4(32 MHz Bandwidth, 8 stream)
	C5(16 MHz Bandwidth, 16 stream)
Max. number of corr./input	120 cross + 16 auto
Sub-array	$2 \operatorname{case}(12+4, 8+8)$
Bandwidth	512 MHz
Max. data rate/antenna	2048 Mbps VSI-H(32 parallels, 64MHz clock)
Max. delay compensation	$\pm~36{,}000~\mathrm{km}$
Max. fringe tracking	$1.075~\mathrm{kHz}$
FFT work length	16+16 bits fixed point for real, imaginary
Integration time	$25.6~\mathrm{msec} \sim 10.24~\mathrm{sec}$
Data output channels	8192 channels
Data output rate	Max. 1.4GB/sec at 25.6msec integration time
a For more details, see the fell	lowing wobsite:

^aFor more details, see the following website:

 $\label{linear_http://kvn.kasi.re.kr/status_report/correlator_status.html} {}^b This mode is available for only KaVA.$

3 Observing Proposal

3.1 Call for Proposals (CfP)

We invite proposals for the open-use observations of EAVN. Please refer to the following EAVN webpages for more details about the array and its performance, and how to prepare and submit a proposal.

This EAVN open-use call is based on risk-share, and provides opportunities of VLBI observations at 22 and 43 GHz for astronomers in the world. If proposers are not familiar with EAVN, they are recommended to include at least one collaborator from EAVN. The contact address for the support is eavnhelp(at mark)kasi.re.kr.

EAVN observations are conducted with single polarization (LHCP) and the data are recorded with the data rate of 1 Gbps. The data obtained at NRO45 and TAK32 are recorded with the data rate of 2 Gbps and reformatted to 1 Gbps data at Mizusawa VLBI Observatory of NAOJ. The total observation time for EAVN is up to 500 hours, while the available observing time for each EAVN telescope is different between each other, as shown in Table 9.

Table 9: Available observing time and frequency for each EAVN telescop	Table 9: Ava	ailable observ	ving time	and frequency	for each	EAVN te	lescope
--	--------------	----------------	-----------	---------------	----------	---------	---------

		1 V		
Array/telescope	Total time [h]			iency
		for one proposal [h]	22 GHz	43 GHz
KaVA	500	_	•	•
Tianma (TMRT65)	100	24	•	•
Nanshan (NSRT26)	100	24	•	
Nobeyama (NRO45)	36	24	•	•
Takahagi (TAK32)	50	24	•	

Special conditions to be considered for EAVN proposal submission are shown below.

- Total telescope time for KaVA is 500 hours. Proposers can request for the KaVA's telescope time with no limitation for one proposal. Note that KaVA is a mandatory array for all EAVN observations.
- Total telescope time for TMRT65 and NSRT26 are 100 hours for each, and proposers can request for the maximum total observation time of 24 hours for each telescope for one proposal.
- Total telescope time for NRO45 is 36 hours, and proposers can request for the maximum total observation time of 24 hours for one proposal. Please include 1-hour additional time for overhead to each observing epoch in NRO45's total request time if your proposal requires NRO45 to join. If your proposal consists of two-epoch observations with the observing time of 8 hours per epoch with NRO45, for example, total request time for NRO45 shall be 18 hours (= (8 + 1) hours ×2 epochs). Available date for EAVN observation with NRO45 is fixed from 2020 December 1 through 2021 January 15. Moreover, NRO45's telescope time is allocated to the slots of consecutive 12 hours or 24 hours.

- Total telescope time for TAK32 is 50 hours, and proposers can request for the maximum total observation time of 24 hours for one proposal. Available date for EAVN observation with TAK32 is fixed from 2020 November 1 through 2021 January 15.
- In the 2020B semester, EAVN accepts a request of usage of subarray configuration (KaVA 4 telescopes and additional telescopes from NRO45, TMRT65, NSRT26, and TAK32), as well as EAVN full array configuration with 8 or 6 telescopes at 22 or 43 GHz, respectively.A proposer shall clarify the reason for the choice of sub-array configuration in the proposal.
- EAVN observations will be scheduled between 1st September 2020 and 15th January 2021.

In summary, non-KaVA telescopes (TMRT65, NSRT26, NRO45, and TAK32) will participate in EAVN observations together with KaVA according to scientific needs and their availability. Note that proposals submitted to EAVN can be assigned to KaVA according to the decision by the EAVN Time Allocation Committee (TAC).

EAVN proposal submission deadline is at

08:00 UT on 15 June, 2020.

Detailed information on the EAVN call-for-proposal can be found in the following webpage:

https://radio.kasi.re.kr/eavn/proposal_info.php

3.2 Proposal Submission

The EAVN proposal application form and proposal submission are available at the EAVN website. If you have any questions regarding to your proposal submission, contact to "eavnprop(at mark)kasi.re.kr". A proposal shall contain the coversheet (two pages), scientific and technical justification including figures and tables (maximum of three pages) with the minimum font size of 10 points. The results of the review will be announced to each PI by early August, 2020².

3.3 Special Condition for Selecting Proposals

All submitted proposals for EAVN are reviewed by referees and the EAVN TAC allocates the observing time based on the referee's rating. A proposal submitted for EAVN observations could be allocated as KaVA observations depending on its rating and the decision made by TAC. Proposers thus should specify the necessity of including non-KaVA telescopes in your observations.

²It might be delayed in case of possible problems in the new corona virus.

3.4 Observation Mode

EAVN provides opportunities of observations at two observing frequencies, 22 and 43 GHz. All EAVN observations are conducted with single polarization (LHCP) and with the data recording rate of 1 Gbps (total bandwidth of 256 MHz). Three types of setup of the digital filter ('C2 mode' with 2 IFs \times 128 MHz, 'C4 mode' with 8 IFs \times 32 MHz, and 'C5 mode' with 16 IF \times 16 MHz) are available, while the C2 mode is not available if your proposal contains requests for usage of non-KaVA stations. The C4 mode is available at both frequencies, while the C5 mode can be used at only 22 GHz. Available observing mode of EAVN is summarized in Tables 10 and 11. This is due to the availability of NRO45, as mentioned in Section 3.1.

Table 10: Available observing mode of EAVN.

		0			
Frequency	$22~\mathrm{GHz}$	43 GHz			
Telescope	KaVA, NRO45, TMRT65,	KaVA, NRO45, TMRT65			
	NSRT26, TAK32	(6 telescopes)			
	(8 telescopes)				
Backend mode	$C2^a$, $C4$, $C5$	$C2^{a}, C4, C5^{b}$			
Recording rate		1 Gbps^c			
Polarization	Left-hand circu	lar polarization (LHCP)			
Correlator	Daejeon Hardware Correlator				

^a C2 mode is available at only KaVA telescopes.

Table 11: Available observing mode for each EAVN telescope.

Telescope	Frequency			Observing mode						
	22 GHz	43 GHz	Total int. ^a	Fast sw. ^b	HB^c	K/Q^d	ToO^e			
KaVA	•	•	•	•	•	•	•			
TMRT65	•	•	•				•			
NSRT26	•		•	•			•			
NRO45	•	•	•							
TAK32	•		•							

^a Total intensity imaging.

3.5 Possible Conflict/Duplication with KaVA/EAVN Large Programs

In order to avoid conflict and/or duplication of the targets with existing KaVA Large Programs (LPs), proposers are highly recommended to visit the KaVA LP webpage where KaVA LPs and their source lists are presented:

https://radio.kasi.re.kr/kava/large_programs.php.

 $[^]b$ C5 mode is available at KaVA and TMRT65.

^c The data obtained at NRO45 and TAK32 are recorded with 2 Gbps and reprocessed to 1 Gbps.

^b Fast antenna switching. See Section 4.1.

^c 1-beam hybrid mode. See Section 4.2.

d K/Q-band simultaneous observation mode. See Section 4.4.

e Target of opportunity. See Section 3.6.

Proposals to be submitted for this opportunity should not have the same scientific goal with LPs, while it is fine to propose same sources with LPs if your proposal has a different scientific goal with LPs.

3.6 Target of Opportunity (ToO) Observations

EAVN accepts ToO proposals. Proposers can request the participation of TMRT65 and NSRT26 as well as KaVA for ToO observations, while both telescopes will join only on a best effort basis. Note that both NRO45 and TAK32 cannot be included for ToO proposals.

It is strongly recommended that ToO proposals (especially expected ToO) are submitted during the regular CfP. Unexpected or urgent ToO can be submitted as Director's Discretionary Time (DDT) proposals. ToO proposals must include clear triggering criteria to initiate an observation. ToOs are valid for one year after it is approved. ToO proposals for DDT should follow the same format of regular call and should be sent to "eavnprop(at mark)kasi.re.kr".

3.7 Angular Resolution and Largest Detectable Angular Scale

The maximum angular resolution for EAVN observations is 0.65 mas at 22 GHz for VERA-Mizusawa – NSRT26 baseline, and 0.70 mas at Q-band for VERA-Mizusawa – Tianma baseline in 2020B. The synthesized beam size strongly depends on UV coverage, and could be higher than the values mentioned above because the baselines projected on UV plane become shorter than the distance between telescopes. The beam size can be calculated approximately by the following formula;

$$\theta \sim 2063 \left(\frac{\lambda}{[\text{cm}]}\right) \left(\frac{B}{[\text{km}]}\right)^{-1} [\text{mas}],$$
 (2)

where λ and B are observed wavelength in centimeter and the maximum baseline length in kilometer, respectively.

The minimum detectable angular scale for interferometers can be also expressed by equation (2), where the baseline length B is replaced with the shortest one among the array. Because of the relatively short baselines provided by KVN, ~ 300 km, KaVA is able to detect an extended structure up to 9 mas and 5 mas for the K- and Q-bands, respectively.

As for an EAVN array in which non-KaVA stations (except NSRT26) are added to KaVA, the longest/shortest baselines remain the same as those of KaVA. The maximum angular resolutions and the largest detectable angular scales are thus basically the same, although their detailed values in a synthesized image are dependent on the scheme of UV weighting as well as the UV coverage. As for an EAVN array which additionally includes NSRT26 at K-band, the longest baseline length extends to 4375 km (primarily along the east-west direction). This enhances the maximum angular resolution at K-band by a factor of ~ 3 compared to that of KaVA in 2020B.

3.8 Sensitivity

TAK32

40

0.4

When a target source is observed, a noise level $\sigma_{\rm bl}$ for each baseline can be expressed as

$$\sigma_{\rm bl} = \frac{2k}{\eta} \frac{\sqrt{T_{\rm sys,1} T_{\rm sys,2}}}{\sqrt{A_{e1} A_{e2}} \sqrt{2B\tau}} = \frac{1}{\eta} \frac{\sqrt{SEFD_{\rm sys,1} SEFD_{\rm sys,2}}}{\sqrt{2B\tau}},\tag{3}$$

where k is Boltzmann constant, η is quantization efficiency (~ 0.88), $T_{\rm sys}$ is system noise temperature, SEFD is system equivalent flux density, A_e is antenna effective aperture area ($A_e = \pi \eta_A D^2/4$ in which A_e and D are the aperture efficiency and antenna diameter, respectively), B is the bandwidth, and τ is on-source integration time. Note that for an integration time beyond 3 minutes (in the K-band), the noise level expected by equation (3) cannot be attained because of the coherence loss due to the atmospheric fluctuation. Thus, for finding fringe within a coherence time, the integration time τ cannot be longer than 3 minutes. For VLBI observations, signal-to-noise ratio (S/N) of at least 5 and usually 7 is generally required for finding fringes.

A resultant image noise level $\sigma_{\rm im}$ can be expressed as

$$\sigma_{\rm im} = \frac{1}{\sqrt{\Sigma \sigma_{\rm bl}^{-2}}}. (4)$$

If the array consists of identical antennas, an image noise levels can be expressed as

$$\sigma_{\rm bl} = \frac{2k}{\eta} \frac{T_{\rm sys}}{A_e \sqrt{N(N-1)B\tau}} = \frac{1}{\eta} \frac{SEFD}{\sqrt{N(N-1)B\tau}},\tag{5}$$

where N is the number of antennas. Using the typical parameters shown in Table 12, baseline and image sensitivity values of EAVN can be calculated as listed in Tables 13 and 14 (baseline and image sensitivities of KVN, VERA, and KaVA, as well as EAVN, are also shown for reference). Table 13 contains all combinations of baselines, while Table 14 indicates part of possible combinations of telescopes.

Station		K-band			Q-band			
	$T_{\rm sys}$ [K]	$\eta_{ m A}$	SEFD [Jy]	\overline{I}	$T_{\rm sys}$ [K]	$\eta_{ m A}$	SEFD [Jy]	
KVN	100	0.6	1328		150	0.6	1992	
VERA	120	0.5	2110		250	0.5	4395	
TMRT65	60	0.5	100		66	0.5	110	
NSRT26	42	0.6	364		_	_	_	
NRO45	100	0.61	285		200	0.53	655	

343

Table 12: Parameters of each telescope.

Figures 16 and 17 show the system noise temperature at Mizusawa and Ulsan, respectively. For Mizusawa, receiver noise temperatures are also plotted.

Note that the receiver temperature of VERA includes the temperature increase due to the feedome loss and the spill-over effect. In Mizusawa, typical system temperature in the K-band is $T_{\rm sys}=150$ K in fine weather of winter season, but sometimes rises

Table 13: Baseline sensitivity of EAVN.

	K-band							Q-1	band	
	KVN	VERA	TM65	NRO45	NS26	TAK32	KVN	VERA	TM65	NRO45
KVN	6.1	7.7	1.7	2.8	3.2	3.1	9.1	13.6	2.2	5.2
VERA	_	_	2.1	3.6	4.1	3.9	_	_	3.2	7.8
TMRT65	_	_	_	0.8	0.9	0.8	_	_	_	1.2
NRO45	_	_	_	_	1.5	1.4	_	_	_	_
NSRT26	_	_	_	_	_	1.6	_	_	_	_

Note: 1σ baseline sensitivity values are listed in unit of mJy, which assume an integration time of 120 seconds and a bandwidth of 256 MHz for the calculation. In the case of narrower bandwidth of 15.625 KHz (for maser emission), sensitivities can be calculated by multiplying a factor of 128.

Table 14: Image sensitivity of EAVN.

Array	N_{ant}	$N_{\rm bl}$	K-band	Q-band
KVN	3	3	320	480
KaVA	4	6	250	400
KaVA+TMRT65	5	10	80	105
KaVA+NRO45	5	10	120	215
KaVA+TMRT65+NRO45	6	15	50	70
KaVA+TMRT65+NSRT26	6	15	55	_
KaVA+TMRT65+NSRT26+NRO45	7	21	40	_
KaVA+TMRT65+NSRT26+NRO45+TAK32	8	28	32	_

Note: $N_{\rm ant}$ and $N_{\rm bl}$ are the numbers of telescopes and baselines for each array. 1σ image sensitivity values are listed in unit of $\mu \rm Jy$, which assume an integration time of 4 hours and a total bandwidth of 256 MHz for the calculation. In the case of narrower bandwidth of 15.625 kHz (for maser emission), sensitivities can be calculated by multiplying a factor of 128.

above $T_{\rm sys}=300$ K in summer season. The typical system temperature in the Q-band in Mizusawa is $T_{\rm sys}=250$ K in fine weather of winter season, and $T_{\rm sys}=300-400$ K in summer season.

The typical system temperature in the K-band at all KVN stations is around 100 K in winter season. In summer season, it increases up to ~ 300 K. In the Q-band, the typical system temperature is around 150 K in winter season and 250 K in summer season at Yonsei and Tamna. The system temperature of Ulsan in the Q-band is about 40 K lower than the other two KVN stations. This is mainly due to the difference in receiver noise temperature (see Table 5).

3.9 Calibrator Information

The NRAO VLBA calibrator survey is very useful to search for a continuum source which can be used as a reference source to carry out the delay, bandpass, and phase calibrations. The source list of this calibrator survey can be found at the following VLBA homepage,

http://www.vlba.nrao.edu/astro/calib/index.shtml.

For delay calibrations and bandpass calibrations, calibrators with 1 Jy or brighter are strongly recommended as listed in the VLBA fringe finder survey:

http://www.aoc.nrao.edu/~analysts/vlba/ffs.html.

Interval of observing calibrator scans must be shorter than 1 hour to track the delay and delay rate in the correlation process.

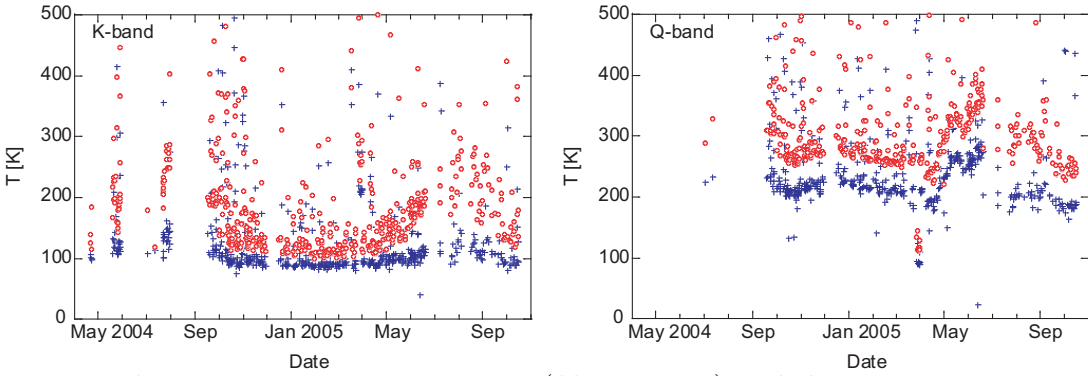


Figure 16: The receiver noise temperature (*blue crosses*) and the system noise temperature (*red open circles*) at the zenith at K-band (left) and Q-band (right) in VERA-Mizusawa station.

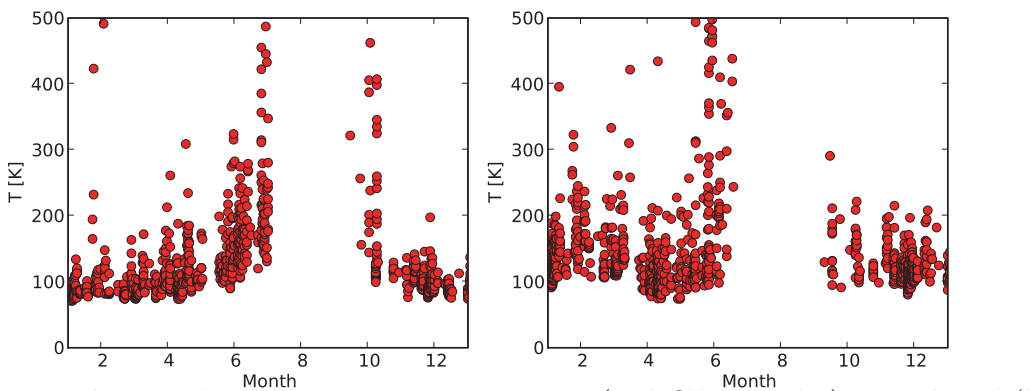


Figure 17: The zenith system noise temperature (red filled circles) at K-band (left) and Q-band (right) in KVN-Ulsan station.

3.10 Data Archive

The users who proposed the observations will have an exclusive access the data for 18 months after the correlation. After that period, all data for EAVN open-use observations will be released as archive data. Thereafter, archived data will be available to any user upon request. This policy is applied to each observation, even if the proposed observation is comprised of multi-epoch observations in this season.

4 Notes for special modes

In this section, we summarize additional information about special observing/data analysis modes.

4.1 Phase-referencing and astrometry

Here, we summarize the maximum capability of EAVN phase-referencing and KaVA astrometry. We note that the number of antennas in VERA is reduced from 4 to 1 which degrade the accuracy of the astrometry as summarized in Appendix.

EAVN is capable of phase-referencing observations to image weak target sources, which cannot be detected within coherent time, and to conduct absolute astrometry measurements. Note that astrometry capability has been confirmed for K-band observations with KaVA 7 telescopes. Although we do not prevent EAVN proposers from submitting proposals with the phase-referencing mode at Q-band and/or with the mode using non-KaVA telescopes within the maximum driving speed of each antenna shown in Table 3, the data quality is not guaranteed.

4.1.1 Fast switching

Fast switching observation with EAVN is recommended for phase referencing (and astrometry) since the verification of the fast switching with EAVN has been finished, except for Tianma 65m, Nobeyama 45m and Takahagi 32m telescopes. In this mode, the antenna nods between phase calibrator (reference) and target source. With this mode, we can detect and image weak sources, which can not be imaged directly by fringe fitting. Regarding antenna switching cycle, users can refer to Table 15.

4.1.2 Separation angle between target and phase reference

It is strongly recommended to observe a pair sources with a small separation angle (e.g., less than 1 degree) at high elevation for precise astrometry. For instance, Martí-Vidal et al. (2010, A&A, 515, 53) demonstrated that the dynamic range of the phase-referenced image is inversely proportional to the sine of the calibrator-to-target separation as

$$D_1 = \left(\frac{\sqrt{\Delta t}}{K\nu}\right) \left(\sin\theta_{\text{sep}}\right)^{-1},\tag{6}$$

where Δt is the on-source observing time, ν , the observing frequency, θ_{sep} , the separation angle between the target and calibrator, and K, a constant to be determined.

4.1.3 Tropospheric calibration with GPS or JMA or Geodetic blocks

Generally, residual of atmospheric zenith delay dominates cm-wave VLBI positional accuracy. Atmospheric (tropospheric) calibration for EAVN has three options (see Table 16), which are (1) GPS, (2) Japan Meteorological Agency (JMA) meso-scale

Table 15:	Phase-R	Referencing	Cycle	Times (min`).*

	0 0						
	Typic	cal weather	Bad	weather	Good weather		
	$(C_n^{\dagger} = 1)$	$2 \times 10^7 \text{ m}^{-1/3}$	$(C_n^{\dagger} = 4)$	$(C_n^{\dagger} = 4 \times 10^7 \text{ m}^{-1/3})$		$\times 10^7 \text{ m}^{-1/3}$	
	Frequ	Frequency (GHz)		Frequency (GHz)		ncy (GHz)	
EL (deg)	22	$(43)^{\ddagger}$	22	$(43)^{\ddagger}$	22	$(43)^{\ddagger}$	
5	0.3	0.2	0.2	0.1	0.8	0.4	
10	0.5	0.3	0.2	0.1	0.8	0.6	
15	0.7	0.3	0.3	0.1	1.5	0.7	
20	0.8	0.4	0.3	0.2	1.8	0.9	
25	0.9	0.4	0.4	0.2	2.0	1.0	
30	1.0	0.5	0.4	0.2	2.8	1.1	
40	1.1	0.5	0.5	0.2	5.8	1.3	
50	1.3	0.6	0.6	0.3	9.9	1.5	
60	1.8	0.7	0.6	0.3	10.0	2.2	
70	2.3	0.7	0.6	0.3	10.0	2.9	
80	2.6	0.7	0.6	0.3	10.0	3.3	

^{*} Referring to Ulvestad, J., Phase-Referencing Cycle Times, VLBA Scientific Memo 20 (1999).

Column 1 shows antenna elevation angles. Columns 2-3 indicate phase-referencing cycles at 22 and 43 GHz, respectively, under typical weather condition. The phase-referencing cycle is defined as the time between the midpoints of the two calibrator observations before and after the target observation. Columns 4-5 are the same as Columns 2-3, but with bad weather condition (similar to some summer days). Columns 6-7 are the same as Columns 2-3, but with good weather condition (similar to some winter nights).

analysis data (Hobiger et al. 2008; JMA 2013¹), and (3) Geodetic blocks². Nagayama et al. (2015, PASJ, 67, 65) and Honma et al. (2008, PASJ, 60, 951) demonstrated that an error of tropospheric zenith delay ($c\Delta\tau_{trop}$) can be suppressed within ~2 cm with GPS, JMA and Geodetic blocks.

Table 16: Tropospheric calibration for each EAVN telescope*.

Telescope	Method							
	GPS	JMA	Geodetic blocks					
KaVA	•	•	•					
TMRT65	\triangle	•	•					
NSRT26	\triangle	×	•					

^{*} TMRT65 = Tianma 65m. NSRT26 = Nanshan 26m. \bullet = Available. \triangle = It would be available in the near future. \times = Not available.

4.1.4 Astrometric accuracy

We have verified astrometric accuracy with KaVA and EAVN, based on (1) a Galactic line source and (2) QSO pair observations (see Figures 18 and 19, and Tables 17 and 18). However, we note that the number of antennas in VERA is reduced from 4 to 1 which degrade the accuracy of the astrometry as summarized in

^{\dagger} C_n is strength of the tropospheric turbulence.

[‡] Now, Q-band phase-referencing mode is under evaluation.

¹http://www.jma.go.jp/jma/jma-eng/jma-center/nwp/outline2013-nwp/pdf/outline2013_ all.pdf

²http://bessel.vlbi-astrometry.org/tech

Appendix. Based on Reid & Honme (2014, ARA&A, 52, 339), single-epoch (relative) astrometric error consists of (1) thermal and (2) systematic errors as shown below:

$$\Delta\theta_{\text{therm}} \approx 12 \left(\frac{\lambda[\text{cm}]}{1.3}\right) \left(\frac{B[\text{km}]}{2,300}\right)^{-1} \left(\frac{\text{S/N}}{20}\right)^{-1} [\mu \text{as}],$$
 (7)

and

$$\Delta s_{\rm rel} \approx 31 \left(\frac{{\rm c}\Delta \tau [{\rm cm}]}{2}\right) \left(\frac{B[{\rm km}]}{2,300}\right)^{-1} \left(\frac{\theta_{\rm sep}[{\rm deg}]}{1}\right) [\mu {\rm as}],$$
 (8)

where λ is the observing wavelength, B, the longest baseline length, S/N, signal-to-noise ratio of (phase-referenced) image, $c\Delta\tau$, the speed of light multiplied by delay residual, and $\theta_{\rm sep}$, separation angle between target and calibrator (phase reference).

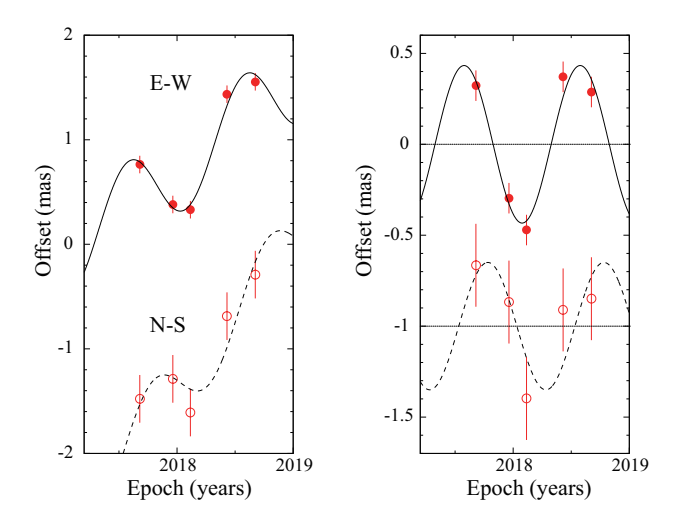


Figure 18: Results of parallax and proper-motion fitting. Plotted are position offset of maser spot (W3(OH) at $V_{\rm LSR} = -47.5~{\rm km~s^{-1}}$) with respect to the background QSO J0244+6228 (with a separation angle of **2.2 degrees**) toward the east (R.A.cos σ) and north (σ) as a function of time. For clarity, the north direction data is plotted offset from the east direction data. (*Left*) The best-fit models in the east and north directions are shown as continuous and dashed curves, respectively. (*Right*) Same as the Left, but with proper motions removed.

Table 17: Parallax results for $W3(OH)^*$.

Array	Frequency	Source	$V_{ m LSR}$	Parallax	$\sigma_{\alpha \cos \delta}^*$	σ_{δ}^*	Ref.
	GHz		${\rm km~s^{-1}}$	(mas)	(mas)	(mas)	
KaVA	22	W3OH	-47.5	$0.460{\pm}0.035$	0.052	0.256	
VLBA	22	W3OH	$-51.5 \sim -48.2$	$0.489 {\pm} 0.017$	$\sim \! 0.050$	$\sim \! 0.050$	(1)

^{*}Positional errors in right ascension and declination were adjusted so that the reduced chi-square becomes unity. Columns 1-2 represent array and observing frequency. Columns 3-4 show source name and LSR velocity of the maser spot, used for the parallax fit. Column 5 displays the parallax result in milli-arcseconds (mas). Columns 6-7 represent the (systematic) positional errors in right ascension and declination, respectively.

Ref. (1) Hachisuka et al. (2006).

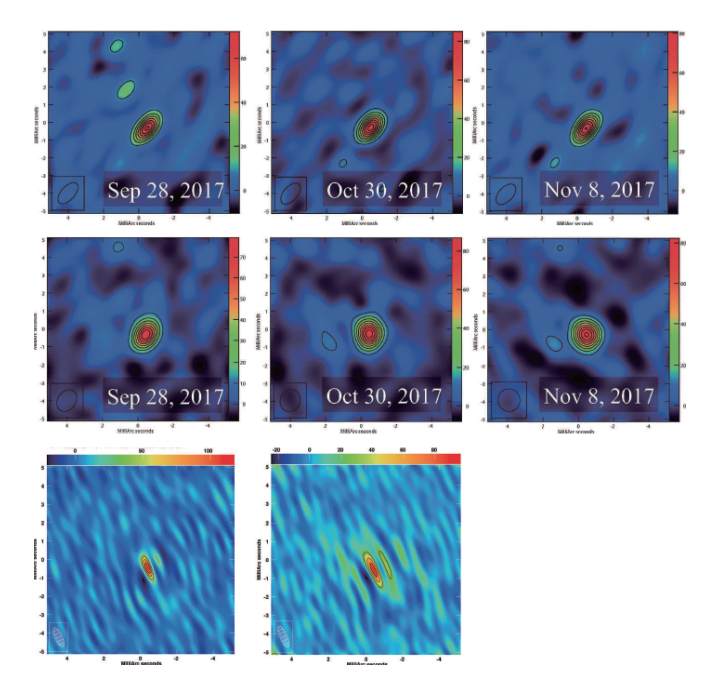


Figure 19: (**Top row**) Phase-referenced images of 0556+238 with VERA, relative to the phase reference 0601+245. The dates of the observations are Sep 28, Oct 30 and Nov 8 in 2017 from left to right. (**Middle row**) Same as the top row, but for KaVA data used. (**Bottom row**) Same as the top row, but for EAVN data used. Observation dates are Mar 27 and May 24 in 2019 from left to right.

4.1.5 Baseline length

The longest baseline length is related to astrometric accuracy as shown in Equations (7) and (8). Baseline lengths for EAVN astrometry are compiled in Table 19.

4.1.6 A priori model of the KJCC correlator

The initial delay tracking model at the KJCC correlator is not sufficient for high precision position measurement. Therefore, we provide a calibration table (called as the delay re-calculation table) to PIs, where the necessary information such as the latest station coordinates, the most-updated Earth-rotation parameters, tropospheric and ionospheric delays is included. The table can be loaded with the AIPS task "TBIN".

For this the delivery of data and calibration table will take about three months after the observation.

4.1.7 Data reduction

Generally, users are encouraged to carry out data reduction in consultation with contact person and/or support scientist in the KaVA/EAVN project group. Procedure of astrometric data reduction for VERA data has been summarized in previous papers (e.g. Fig. 11 of Kurayama et al. 2011; Fig. 5 of Imai et al. 2012). Basically, the procedure of data reduction for KaVA/EAVN data is consistent with that for VERA data, expect for few points.

Table 18: Results of position repeatability for 0556+238.

		1	1	v		
	VE	ERA	Ka	VA	EA	VN
Observation date	R.A.	Decl.	R.A.	Decl.	R.A.	Decl.
	(μas)	(μas)	(μas)	(μas)	(μas)	(μas)
2017/Sep/28	-465 ± 15	-332 ± 16	-451 ± 15	-331 ± 15	_	_
2017 Oct / 30	-494 ± 11	-283 ± 12	-462 ± 16	-258 ± 18	_	_
2017/Nov/8	-505 ± 09	-318 ± 10	-480 ± 13	-287 ± 14	_	_
2019/Mar/27	-463 ± 21	-343 ± 24	-464 ± 14	-336 ± 17	-407 ± 11	-455 ± 21
2019/May/24	-576 ± 85	-479 ± 150	-592 ± 29	-434 ± 35	-411 ± 24	-524 ± 44
Unweighted mean	-500 ± 21	-351 ± 34	-490 ± 26	-330 ± 30	-409 ± 2	-490 ± 35

Column 1 shows the date of observation. Columns 2-3 display image positions of 0556+238 relative to 0601+245 in right ascension and declination, respectively. Note that the image positions were measured for VERA data. The errors of the positions represent the thermal error. Columns 4-5 are the same as the Columns 2-3, but for KaVA data used. Columns 6-7 are the same as the Columns 2-3, but for EAVN data used.

Table 19: Baseline lengths for EAVN astrometry.*

	MIZ	IRK	OGA	ISG	KYS	KUS	KTN	T6	UR
MIZ									
IRK	1,300								
OGA	1,300	1,300							
ISG	2,300	1,000	1,800						
KYS	1,200	700	1,800	1,500					
KUS	1,100	400	1,500	1,300	300				
KTN	1,500	400	1,700	1,000	500	400			
T6	2,000	900	2,100	800	900	900	600		
UR	4,500	4,000	5,200	4,000	3,400	3,700	3,600	3,300	

^{*} The unit is (km). Each value is rounded off to the (nearest) 10. MIZ=Mizusawa; IRK=Iriki; OGA=Ogasawara; ISG=Ishigaki-jima; KYS=Yonsei; KUS=Ulsan; KTN=Tamna; T6=Tianma 65m; UR=Nanshan 26m.

For instance, parallactic angle should be corrected if the fast switching observation is conducted with single beam. The NRAO AIPS task "CLCOR" can be used for the calibration by setting the OPCODE = "PANG".

4.2 1-beam hybrid (K/Q/W) mode

KaVA will enable us to conduct VLBI observations in combinations of different types of antennas (antenna beams), receiving bands, recording rates (namely total band widths), and filtered base band channels in one observing session, whose cross correlation is still valid for the whole or some parts of KaVA. In such "hybrid" observing modes with KaVA, there are some modes that are available in the 2019B CfP described as follows.

Although VERA shall use only one of dual beams in a single frequency band (K or Q), the KVN is able to observe in two to three of K/Q/W bands simultaneously in a common observing session. Please check the KVN status report for W-band information (http://radio.kasi.re.kr/kvn/status_report_2019). Signal correlation for all the KaVA baselines is valid for the band in which both the KVN and VERA ob-

serve, while that for all the observed bands is valid for the KVN baselines.

Frequency allocations should be made separately to the KVN and VERA, including base band channels that are common between the two arrays in a specific band (K or Q). Note that the number of base band channels or the total bandwidth available per frequency band is limited, therefore brighter continuum sources should be selected for group-delay calibration.

4.3 Wide-field imaging mode

This wide-field imaging (WFI) mode was open in the semester 2018A as the KaVA open-use, mainly for to fully image 44 GHz methanol maser emissions associated with star-forming regions, which are generally distributed on the angular scale over 10 arcsec. In this semester 2020B, however, this WFI mode has been decided to be temporarily closed due to reducing the number of radio telescopes in the KaVA this time.

This mode will be opened again after completing verification with the EAVN.

4.4 Simultaneous K/Q band mode

From this semester, simultaneous K/Q band observation with KaVA and NRO45 is available on a limited basis for an open-use. Please note following conditions: (1) All observing time will be allocated during a specific campaign period (e.g., approximately one week) in order to install and uninstall a quasi-optical system at Mizusawa telescope. Hence, multiple monitoring observations cannot be supported. (2) The frequency setup is fixed as shown in Table 20. (3) Frequency phase transfer (FPT) technique [10] is not applicable to the data obtained at NRO45. (4) 'Template method' for the amplitude calibration should be employed to the data obtained at NRO45 since the system noise temperature cannot be measured using the K/Q-band simultaneous reception system at Nobeyama.

Table 20: Frequency setup for simultaneous K/Qvband observation

		, ,	
Band	Frequency range	BBC channel	Polarization
K-band	22.112 - 22.240 MHz	32 MHz x 4 channels	LHCP
Q-band	42.812 - 42.940 MHz	$32~\mathrm{MHz} \ge 4~\mathrm{channels}$	RHCP

A demonstrative observation and detailed performance of simultaneous K/Q-band observations with KaVA is presented in the Zhao et al. (2019). You can also check science cases with simultaneous multi-frequency VLBI observations in the Dodson et al. 2017.

5 Observation and Data Reduction

5.1 Preparation of an EAVN Observation

After the acceptance of proposals, users are requested to prepare the observing schedule file two weeks before the observation date. The observer is encouraged to consult a contact person in the EAVN Array Operation Center (AOC) and/or the assigned support scientist to prepare the schedule file under the support of the contact person and/or the assigned support scientist. The schedule submission should be done by a stand-alone vex file. The examples of EAVN vex file are available at the EAVN web site:

http://radio.kasi.re.kr/kava/kava_observing_preparation.php

Detailed information about preparation and submission of a schedule file for TMRT65 and NRO45 will be announced when distributing the proposal review results.

On your schedule, we strongly recommend to include at least two fringe finder scans, each lasting 5 or more minutes at the first and latter part of observation in order to search the delay and rate offsets for the correlation.

For EAVN which includes the large telescopes (TMRT65 and NRO45), regular pointing check is necessary at both 22 and 43 GHz. You should leave a 8-15 min gap every $\leq 1-2$ hr in your schedule file to allow this. Pointing check is done by the local operators. In addition, we strongly recommend to include frequent scans of a maser source and/or a bright compact continuum source located within 15° from the target. This allows a cross check of the amplitude calibration for TMRT65 and NRO45 along with the usual a priori method.

We request PIs to specify their correlation parameters at the beginning of the vex file for proper correlation processing. In particular, PIs who request for sub-array or dual-beam observations for EAVN should provide a frequency matching table for the correct correlation.

5.2 Observation and Correlation

EAVN members take full responsibility for observation and correlation process, and thus basically proposers will not be asked to take part in observations or correlations. Observations are proceeded by operators from each array and telescope, and correlated data is delivered to the users in approximately two months including the time for media shipping to KJCC at Daejeon.

After the correlation, the user will be notified where the data can be downloaded by e-mail. After one month later of a correlated data distribution to PIs, disk modules which contains raw observing data can be recycled without notice. Therefore, PIs should investigate the correlated output carefully. For re-correlation or raw data keeping of the data, PI should provide adequate evidence in order to justify his/her request. If there is an issue related to correlated data, PI should consult a support scientist first or the correlator team (kjcc (at-mark) kasi.re.kr), and not to ask KJCC members directly.

5.3 Data Reduction

For EAVN data reduction, the users are encouraged to reduce the data using the NRAO AIPS software package. The observation data and calibration data will be provided to the users in a format which AIPS can read.

As for the amplitude calibration, we will provide "ANTAB" files which include the system temperature information measured by the R-sky method and the information of the dependence of aperture efficiency on antenna elevation. If the user wants weather information, the information of the temperature, pressure, and humidity during the observation can be provided.

At present, EAVN does not support astrometric observations. In case of questions or problems, the users are encouraged to ask the contact person in EAVN members and/or the assigned support scientist for supports.

5.4 Further Information

The users can contact any staff member of EAVN by e-mail (see Table 21). Note that your EAVN proposal should be submitted to the following EAVN proposal submission site.

https://radio.kasi.re.kr/eavn/proposal_info.php

Table 21: Contact addresses Name E-mail address Related Field Proposal-related requests/questions Inquiry about eavnprop (at-mark) kasi.re.kr proposal submission User support team eavnhelp (at-mark) kasi.re.kr User support in general Operation team eavnobs (at-mark) kasi.re.kr Observation-related requests/questions, schedule submission Correlator team kjcc (at-mark) kasi.re.kr Correlation-related requests/questions, correlated data distribution

A Effect of the reduction of the VERA antennas

In the 2020B semester, the number of VERA antennas will be reduced from 4 to 1, and the Iriki, Ogasawara, and Ishigakijima stations will not be available for the common use. We evaluate the possible effects on the performance of EAVN by employing the same array configuration available in 2020B (i.e. EAVN without VERA Iriki, Ogasawara, and Ishigakijima stations). For this purpose, we present two cases of imaging simulation with KaVA (masers) and EAVN (AGN) data. In addition, we evaluate performance of astrometry of the H₂O maser source with KaVA.

A.1 Case 1: KaVA imaging of H₂O masers in high-mass starforming region

First, we tested imaging of the KaVA observational data for the 22 GHz H₂O masers. The observation was done as the KaVA Large Program for high-mass star-formation studies (unpublished results). The observation was carried out with the full KaVA array with 7 antennas in a single horizon-horizon track by switching four maser sources every 10 minutes. Calibrations were done by using all the data, but three of the VERA stations (except Mizusawa) were all flagged out in the imaging processes. We present results of two sources in the southern and northern hemisphere at the declination of -33 degrees and +37 degrees for comparison.

Figure 20 show UV coverages of the two sources with/without 3 VERA stations and the resultant beam patterns are presented in Figure 21. The beam sizes, aspect ratios, and side-lobe levels are listed in Table 22. The resolutions become worth by a factor of \sim 2, and the aspect ratios (elongation of the beam) are also factor of \sim 2 larger for the antenna configurations in 2020B (4 antennas) than those of the full array. The sidelobe levels measured by the ratios of the first side lobe levels with respect to the main lobe, are higher by a factor of >2.

We also compared the synthesis images of the selected maser spots at arbitral channels, as shown in Figure 22. We note that the imaging parameters for the masers, such as noise levels, peak intensity, dynamic range, and signal-to-noise ratios strongly depend on the structures of the maser spots and observation conditions (weather condition), rather than the array configuration. Thus, the present results are just for reference. The peak intensities for both maser sources are slightly larger for the 4 antenna array than those of the full array. This is probably because the masers are spatially extended and the longer baselines would have missing flux. Similarly, the rms noise levels seem to be better for the 4 antenna array than those of the full array. This could be explained due to the different beam size and/or higher system noise temperatures in the stations flagged out in the imaging. As for the dynamic range, the results for the northern source is relatively high due to the stronger maser emission. Although the Mizusawa stations show slightly higher Tsys (~100-600 K) than those in other VERA stations ($\sim 200-300$ K), they are all higher than in the KVN stations $(\sim 100 \text{ K})$. Thus, comparison of Table 23 do not readily suggest that the reduction of the KaVA antenna has no effect on the imaging capability.

Table 22: Resolution and sidelobe levels

	$\theta_{ m maj}$	$\theta_{ m min}$	$\sqrt{\theta_{ m maj} \theta_{ m min}}$	PA	$\theta_{ m maj}/\theta_{ m min}$	Sidelobe	
Array	(mas)	(mas)	(mas)	(deg)		Level	
Southern source ($\delta = -3$	Southern source ($\delta = -33$ degrees)						
Full array (7 antennas)	2.44	1.07	1.62	-4.24	2.28	0.256	
2020B (4 antennas)	5.50	1.22	2.59	-12.94	4.51	0.573	
Northern source ($\delta = +37 \text{ degrees}$)							
Full array (7 antennas)	1.22	1.08	1.15	65.06	1.13	0.172	
2020B (4 antennas)	3.04	1.33	2.01	-6.90	2.29	0.454	

Table 23: Imaging parameters for masers

Array	I_{\max}	I_{\min}	$I_{\rm rms}$ (peak)	$I_{\rm rms}$ (line-free)	DR	SNR	
Southern source ($\delta = -33$ degrees)							
Full array (7 antennas)	14.40	-0.56	0.09	0.022	25.57	168.24	
2020B (4 antennas)	19.20	-0.61	0.06	0.017	31.41	333.73	
Northern source ($\delta = +37 \text{ degrees}$)							
Full array (7 antennas)	111.31	-8.34	1.35	0.021	13.35	82.33	
2020B (4 antennas)	129.22	-7.18	0.91	0.011	18.01	141.77	

 $I_{\text{max/min/rms}}$ are in unit of Jy beam⁻¹. Note the differences in beam size.

DR means the dynamic range ($|I_{\text{max}}/I_{\text{min}}|$).

SNR means the signal-to-noise ratio $(I_{\text{max}}/I_{\text{rms}}(\text{peak}))$.

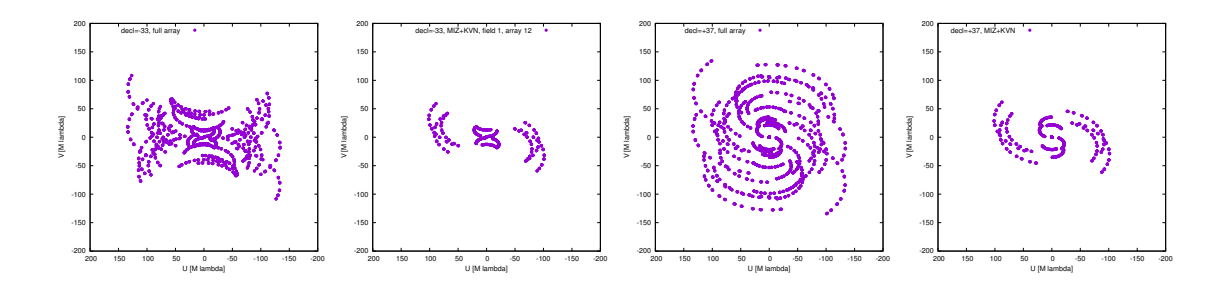


Figure 20: UV coverages. From left to right; full-array for the southern source, four antenna array in 2020B for the southern source, . full-array for the northern source, and four antenna array in 2020B for the northern source.

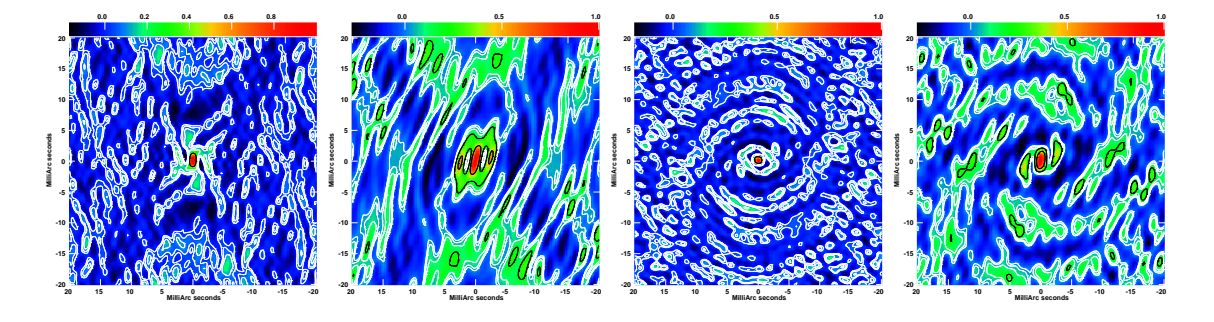


Figure 21: Beam patterns. From left to right; full-array for the southern source, four antenna array in 2020B for the southern source, . full-array for the northern source, and four antenna array in 2020B for the northern source. Contour levels are 2, 5, 10, 20, and 50% of the peak intensity.

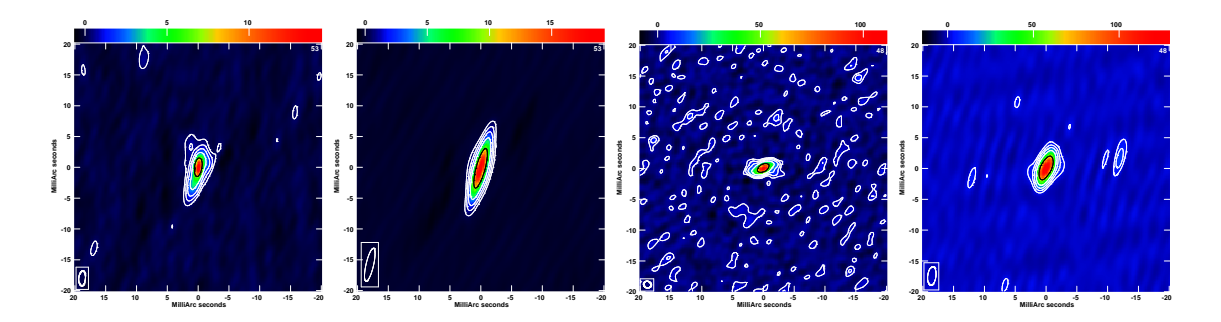


Figure 22: Examples of the maser images. From left to right; full-array for the southern source, four antenna array in 2020B for the southern source, . full-array for the northern source, and four antenna array in 2020B for the northern source. Contour levels are 2, $5,\ 10,\ 20,\ and\ 50\%$ of the peak intensity.

A.2 Case 2: KaVA Imaging of a Continuum Source

In principle a variety of array configurations are possible to examine the impact on EAVN imaging for continuum sources. Here we only consider a representative case, where we compare imaging at 43 GHz between the full-KaVA array and KVN+Mizusawa. We made a simple imaging test by using an actual KaVA observation data that was taken in the past as part of the KaVA AGN Large Program. A radio source M87 was used for this test, which shows a typical core-jet structure for extragalactic nonthermal continuum radio sources. The observation was performed lasted for 5 hours at a recording late of 1 Gbps.

Figure 23 shows the results of image comparison between KaVA and KVN+Mizusawa along with the corresponding uv-coverage plots. Also in Table 24 we summarize some of the image parameters that are relevant to evaluate the image quality. The panel (c) in Figure 23 shows a full-KaVA image of the source that serves as the reference in our test. The panel (d) in Figure 23 shows an image obtained by the array without Iriki, Ishigakijima and Ogasawara. All the images were produced using a natural-weighting scheme.

One can see the following impacts: (1) north-south angular resolution was degraded by a factor of >2 due to the loss of north-south baselines; (2) image-noise levels were increased by a factor of >2 (and the imaging dynamic range was decreased by a factor of 2 or more) due to the degrade of uv-coverage.

The example presented here may be used as a guideline for EAVN-2020B proposal planning on continuum source imaging. One might foresee a similar level of impact at 22 GHz. The addition of other stations (Tianma, Nanshan, Takahagi, Nobeyama) should improve the situation.

Table 24: Image parameters on a continuum source

	Beam size*	$I_{\mathrm{peak}}**$	$I_{\rm rms}$ ***	$I_{ m peak}/I_{ m rms}$
Array	(mas, mas, deg)	(mJy/beam)	(mJy/beam)	
KaVA (7 antennas)	$0.68 \times 0.56, -22$	1180	0.85	1388
KVN+Miz (4 antennas)	$1.86 \times 0.64, -22$	1470	2.47	595

Notes: *: A natural weighting scheme is applied. **: Map peak intensity. ***: Off-core rms image noise level.

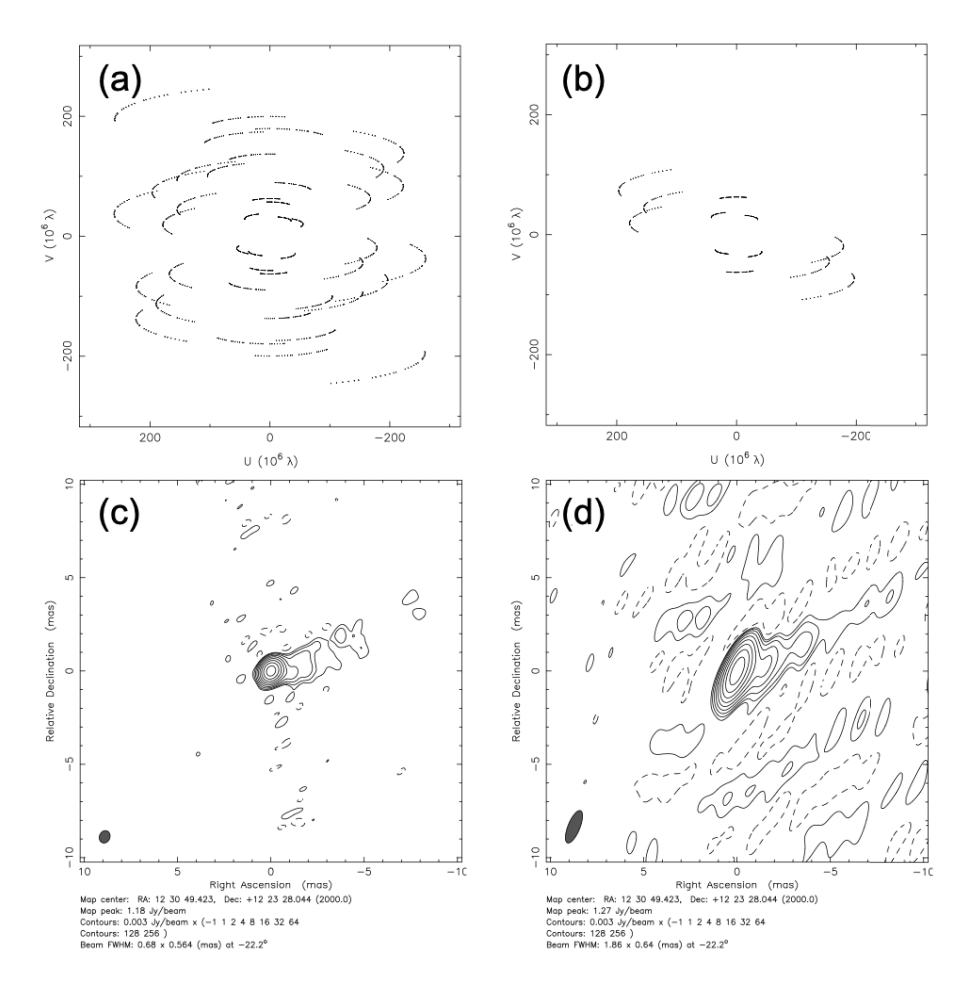


Figure 23: (a) Example uv-coverage of M87 43 GHz with KaVA 7 stations. (b) Example uv-coverage of M87 43 GHz with KVN+Mizusawa 4 stations. (c) M87 43 GHz image with KaVA 7 stations. (d) M87 43 GHz image with KVN+Mizusawa 4 stations. The same contour levels (3 mJy \times -1,1,2,4,8...256) are used in (c) and (d).

A.3 Case 3: KaVA and EAVN astrometry

As shown in Table 19, the longest baseline length of KaVA (EAVN) changes from 2,300 (5,200) km to 1,500 (4,500) km due to the reduction of the VERA antennas. Since astrometric accuracy improves as the longest baseline length (see Equations 7 and 8), KaVA (EAVN) astrometric accuracy would be degraded.

Using previous EAVN data shown in Table 18, we have simulated the effect of the reduction of VERA antennas. Although it is not straight forward to see the result of the simulation, we have tentatively confirmed two possible effects (see Table 25): (1) degrade of thermal error (on the first epoch) and (2) degrade of astrometric accuracy in east-west direction (see the standard error of the unweighted mean). The latter effect could be due to the fact that the longest baseline length between Ogasawara 20m and Tianma 65m cannot be used.

Table 25: Results of position repeatability for 0556+238.

rable 20. Results of position repeatability for 6666 + 266.						
	EA	VN	EAVN	EAVN w/o VERA stations		
Observation date	R.A.	Decl.	R.A.	Decl.		
	(μas)	(μas)	(μas)	(μas)		
2019/Mar/27	-407 ± 11	-455 ± 21	$-400 \pm$	$15 -529 \pm 38$		
2019/May/24	-411 ± 24	-524 ± 44	$-418 \pm$	$24 -536 \pm 43$		
Unweighted mean	-409 ± 2	-490 ± 35	$-409 \pm$	-533 ± 4		

Column 1 shows the date of observation. Columns 2-3 display image positions of 0556+238 relative to 0601+245 in right ascension and declination, respectively. Note that the image positions were measured for EAVN data. The errors of the positions represent the thermal error. Columns 4-5 are the same as the Columns 2-3, but with VERA stations (IRK, OGA, ISG) removed.

References

- [1] KaVA Status Report for 2020B: https://radio.kasi.re.kr/kava/status_report20b/node3.html
- [2] NRO web site: http://www.nro.nao.ac.jp/~nro45mrt/html/index-e.html
- [3] Cho, I. et al. 2017, PASJ, 69, 87
- [4] Han, S.-T., et al. 2008, Int. J. Infrared Millimeter Waves, 29, 69
- [5] Han, S.-T., et al. 2013, PASP, 125, 539
- [6] Lee, S.-S., et al. 2015, JKAS, 48, 229
- [7] Oh, S.-J., et al. 2011, PASJ, 63, 1229
- [8] Oyama, T. et al. 2016, PASJ, 68, 105
- [9] Yonekura, Y., et al. 2016, PASJ, 68, 74
- [10] Zhao, G. Y., et al. 2019, JKAS, 52, 23